3D shell model for the thermo-mechanical analysis of FGM structures via imposed and calculated temperature profiles

3D shell model for the thermo-mechanical analysis of FGM structures via imposed and calculated temperature profiles

S. Brischetto* and R. Torre

Department of Mechanical and Aerospace Engineering, Politecnico di Torino, Torino, Italy

Abstract

The exact three-dimensional (3D) shell model proposed in the present paper is able to perform the thermal stress analysis of simply-supported Functionally Graded Material (FGM) spherical and cylindrical shells, cylinders and plates. The model is based on the 3D equilibrium equations for spherical shells developed using an orthogonal mixed curvilinear coordinate system. The use of this reference system allows the investigation of cylindrical shells, cylinders and plates as particular cases of spherical shells by means of simple considerations on the radii of curvature. The 3D shell model uses a layer-wise approach and the exponential matrix method to calculate the general and the particular solutions through the thickness direction z. The system of second order differential equations in z is not homogeneous because of the thermal terms which are externally defined. The system is reduced to a group of first order differential equations in z simply redoubling the number of variables. The solution is in closed form in the in-plane directions α and β because of the hypotheses of simply-supported boundary conditions, harmonic forms for displacement and temperature fields, and isotropic behavior in the in-plane directions for functionally graded materials. In order to define the equivalent thermal load, the temperature profile through the thickness is separately defined by means of three possible ways. Using the hypothesis of temperature amplitudes imposed at the top and bottom external surfaces in steady-state conditions, the temperature profile can be: imposed as linear through the entire thickness direction, calculated by solving the 1D version of the Fourier heat conduction equation, or calculated by solving the 3D version of the Fourier heat conduction equation. The effects of different temperature profiles on the displacement and stress analyses of FGM plates and shells are here remarked. The first order differential equation system in z has not constant coefficients because of the presence of radii of curvature for shells and through-the-thickness variable elastic and thermal coefficients for the FGM layers. An appropriate number of mathematical layers is introduced to calculate the curvature influence for shells and the elastic and thermal material coefficients for FGM layers. Therefore, the system can be considered as differential equations with constant coefficients. The proposed results allow the evaluation of thickness ratio, geometry, lamination scheme, thickness material law and temperature profile effects in the related thermal stress analysis of single-layered and sandwich FGM plates, cylinders, spherical and cylindrical shells.

Keywords: 3D exact shell solution; linear assumed temperature profile; 1D and 3D Fourier heat

*Author for Correspondence: Salvatore Brischetto, Department of Mechanical and Aerospace Engineering, Politecnico di Torino, corso Duca degli Abruzzi 24, 10129 Torino, ITALY. tel: +39.011.090.6813, fax: +39.011.090.6899, e.mail: salvatore.brischetto@polito.it.

conduction equation; functionally graded plates and shells; thermal stress analysis.

1 Introduction

Functionally Graded Materials (FGMs) are a particular group of advanced composite materials where two or more constituent phases are continuously graded over a defined volume. FGMs are heterogeneous materials which have graded elastic and thermal properties. This variation can be unidirectional or multidirectional, and it allows to achieve optimized characteristics for each structure. FGMs commonly employed in the aerospace field are continuously graded in one particular direction, usually the thickness direction, and they represent a valid alternative to classical composite materials because of the elimination of interface problems between two adjacent layers [1]. High-temperature structures are typical of the aerospace field because of the severe thermal environment conditions. FGMs can tolerate high temperatures, in particular when their configurations are a combination of a ceramic and a metallic phase. FGMs can have a fundamental role in the decrease of thermal stresses. Aerospace applications are influenced by the recent developments in the field of composites: high strength-to-weight, thermal resistance and wear resistance are fundamental features when FGMs are compared with conventional materials. The selection of materials in aerospace industry is based on mechanical and thermal properties, and also on cost advantages [2]. High temperatures, high temperature gradients and cyclical changes of temperature are typical conditions in supersonic and high-altitude airplanes, space shuttles, launch vessels and advanced propulsion systems [3]- [5]. In these applications, an appropriate thermal stress analysis is a fundamental point, in particular in the case of plate and shell structures embedding FGM layers [5], [6]. In the thermo-mechanical investigation of these structures, the development of an efficient elastic model and the rigorous determination of a correct temperature profile are equally important. In the case of FGM layers, the analysis is further complicated by the continuous variation in the thickness direction of both elastic and thermal properties. The mechanical model can be based on a numerical or analytical 3D, 2D or 1D approach. The equivalent thermal load is strictly connected with an appropriate definition of the temperature field by means of a linear assumed temperature profile through the entire thickness of the structure or the resolution of the 1D or 3D version of the Fourier heat conduction equation. Possible alternatives could be the use of a uniform heat flux or the full coupling between the mechanical and thermal fields in order to calculate the temperature profile as a primary variable of the fully coupled thermo-mechanical model [7]- [13].

The new proposed 3D exact shell model has been here developed for the thermal stress analysis of single-layered and sandwich plates and shells embedding FGM layers. This work is the companion paper of the past authors' work [14] about the exact 3D shell thermal stress analysis of structures embedding classical materials or typical composites. The new difficulty here introduced is the inclusion of non-constant elastic and thermal coefficients (which vary through the thickness direction) in the 3D equilibrium equations and in the resolution of the Fourier heat conduction problem (both 1D and 3D versions). The literature review proposed in this introduction remarks the gap present in the state-of-art for a general 3D shell model able to investigate both FGM plates and shells with the possibility of considering several temperature profile types. The discussion of the literature is divided in two main groups: analytical and numerical 3D and 2D models for typical one-layered, multilayered and sandwich structures, and analytical and numerical 3D and 2D models for plates and shells embedding FGM layers. 3D and 2D models for the thermal stress analysis of FGM structures are less numerous.

In the case of typical composite and sandwich structures, the 3D exact solution by Bhaskar et al. [15] was a plate model based on an assumed linear temperature profile. The previous 3D elastic models by Pagano [16]- [18] were extended by Bhaskar et al. [15] using a linear uncoupled thermo-elastic formulation. Further exact 3D plate models were those by: Tungikar and Rao [19], where a useful analytical solution for the calculation of the temperature profile was proposed for the first time, Savoia and Reddy [20], which developed the governing equations in displacement form for a multilayered plate,

and Kulikov and Plotnikova [21] which employed the sampling surface method. The solution of the steady-state form of the three-dimensional Fourier heat conduction equation by Tungikar and Rao [19] for composite plates is also employed in the present paper where it will be extended to FGM shells. 3D exact thermo-electro-mechanical analyses were performed by Kapuria et al. [22], [23] in the case of cylindrical shells by solving the heat conduction problem. Cylindrical shells were also analyzed by Xu and Noor [24] by means of a 3D exact coupled thermo-electro-elastic model where the temperature was directly obtained from the developed model. More general 3D models are the numerical ones as they allow the analysis of boundary conditions different from the simply supported sides, and thermal and mechanical loads different from the harmonic ones. Therefore, Qu et al. [25] developed a 3D Boundary Element Method (BEM) for the thermal stress analysis of plates and shells via a priori assumed quadratic through-the-thickness temperature profile. The 3D BEM analysis by Ochiai et al. [26] for plates and shells employed a 1D calculated temperature profile in place of an assumed temperature profile. Rolfes et al. [27] proposed the thermo-mechanical analysis of composite plates using shell finite elements and they analyzed the temperature via both finite difference methods and 3D finite elements. Other 3D numerical models are based on the fully coupled thermo-elastic theory. Padovan [28] wrote 3D elastic and conduction governing equations for the thermo-mechanical analysis of laminated cylinders. Tanaka et al. [29] proposed a 3D boundary element method for the coupled thermoelastic analysis of a 2D medium using rectilinear coordinates. Thermoelastic frequencies of circular plates were investigated in [30] in the case of free and clamped sides. The Galerkin method was used by Yeh [31] to investigate the coupled thermo-mechanical frequencies of plates. A 3D finite element thermal stress analysis of multilayered composite spherical shells was performed in [32]. Kalogeropoulos et al. [33] used 3D non-linear finite elements for the analysis of extended end-plate steel connections subjected to elevated temperatures. Bîrsan [34] solved the thermal stress analysis of cylindrical elastic shells via Cosserat surfaces. The temperature profile was assumed as general polynomial functions. 2D models have a smaller computational cost than 3D models but they can show some difficulties for thick structures and/or complicated lamination schemes. The separation in 2D analytical and 2D numerical models is here still valid as already seen for the 3D models. Khare et al. [35] proposed an exact 2D higher-order shear deformation theory for the thermal stress analysis of simply supported doubly curved composite multilayered shells using the Sanders theory. The temperature profile was a priori assumed as linear through the entire thickness direction. Ali et al. [36] developed an exact displacement-based higher order plate theory for thick multilayered structures in the case of mechanical and thermal loads. The temperature profile was not calculated but it was a priori assumed. Jonnalagadda et al. [37] proposed the analysis of composite plates using a higher-order displacement field and a linear temperature profile. The state space approach proposed in [38] was used to exactly solve the thermo-elastic governing equations for cylindrical shells in the case of assumed linear or constant temperature profile through the entire thickness direction. In [39], the Reddy displacement theory was added to the model already seen in [38] to analyze new geometries such as spherical shells. The temperature profile was the same used in [38]. Murakami [40] developed an exact solution for the thermal stress analysis of multilayered plates in the case of constant or linear through-the-thickness temperature profile. A shear deformation plate theory was employed. The closed-form global-local higher order model in [41] was used for the thermo-mechanical analysis of shells subjected to constant or linear through-the-thickness temperature profiles. Kapuria et al. [42] used a higher order zigzag theory for the thermal stress analysis of multilayered composite and sandwich beams. The thermal load is defined by means of a linear temperature profile inside each single layer. Refined exact 2D models (in both Equivalent Single Layer (ESL) and Layer Wise (LW) form) were considered in [43]- [49] for the thermal and hygroscopic stress analysis of multilayered composite and sandwich plates and shells. In these works, the temperature and moisture content profiles can be a priori defined as linear through the entire thickness direction or they can be calculated by solving the 3D versions of Fourier heat conduction equation and Fick moisture diffusion law. In [47]- [49], the temperature profile was also obtained as a primary variable

of the problem by means of the fully coupled thermo-electro-elastic analysis. A similar fully coupled thermo-electro-elastic approach was used by Cho and Oh [50] to develop a classical 2D zigzag plate model for smart structures. Assumed temperature profiles were considered in the 2D numerical models proposed in [51] for the thermo-mechanical analysis of shells via a non linear Finite Element (FE) Mindlin theory, in [52] for the thermo-mechanical analysis of multilayered structures via a higher-order beam-type plate model, and in [53] for the thermal stress analysis of multilayered composite plates via classical theories. Jafari et al. [54] proposed the thermo-elastic analysis of plates containing a hole using a constant heat flux. Librescu and Lin [55] employed a linear temperature profile in each layer in the case of a non-linear shear deformable theory for the analysis of plates and shells. Miller et al. [56] developed a Rayleigh-Ritz model based on a classical shell theory for the thermo-mechanical analysis of multilayered cylindrical shells. Cheng and Batra [57] solved the 3D heat conduction problem to develop a third-order numerical shell model for the thermal stress analysis. Rolfes and Rohwer [58] employed the 2D QUAD finite element of Nastran for the analysis of composite plates and shells in the case of a quadratic through-the-thickness temperature profile based on the 3D heat conduction problem. Commercial codes were also used in [59] where the finite element thermo-mechanical analysis was proposed for composite tubes subjected to thermal loads. I-DEAS and ANSYS codes (based on 2D shell or 3D solid elements) were employed. 2D numerical coupled thermo-elastic models were proposed in [60]- [64]. A mixed finite element model for composite plates was given in [60] and [61] by means of a zizag theory and a third-order shear deformation theory, respectively. The finite element analysis was also proposed by Ibrahimbegovic et al. [62] in the framework of a first order shear deformation theory for multilayered shells. Lee [63] developed a numerical model based on the basic equations of thermoelasticity given in polar coordinates for multilayered hollow cylinders. Oh and Cho [64] developed a cubic zigzag three-node triangular finite element plate model where mechanical, thermal and electric fields were fully coupled.

In the case of plates and shells embedding Functionally Graded Material (FGM) layers, the models for the thermo-mechanical analysis of FGM structures are less numerous. The classification in 3D exact, 3D numerical, 2D exact and 2D numerical models is still valid. Among these works, some of the most important ones are discussed in the following part. Reddy and Cheng [65] proposed a 3D exact plate model for FGM structures where the temperature profile was calculated. Alibeigloo and Zanoosi [66] proposed an exact 3D model for the thermo-electro-mechanical analysis of functionally graded carbon nanotube reinforced composite cylindrical shells using governing ordinary differential equations solved via the expansion of variables for axial coordinates and the state space technique for the radial direction. In the exact 3D model by Vel and Pelletier [67], the thermal stress analysis of FGM cylindrical shells was performed via 3D equations in circumferential coordinates and the resolution of both 1D and 3D Fourier heat conduction equations. The 3D numerical plate model by Adineh and Kadkhodayan [68] used the differential quadrature method and the solution of the 3D version of the heat conduction problem to calculate the temperature profile in FGM layers. A further 3D numerical model was that proposed in [69] where the multifield equations were derived for the thermo-mechanical analysis of FGM shells of revolution embedding piezolectric layers. The thermal buckling of functionally graded cylindrical shells was proposed in [70] via a 2D exact model based on the Donnell shell theory. A linear temperature profile through the thickness was employed. The exact 2D shell model by Pelletier and Vel [71] was developed for the thermo-mechanical analysis of FGM cylindrical shells. The 3D Fourier heat conduction equation was solved to obtain the correct temperature profile. Refined ESL and LW 2D models in exact form were developed in [72] and [73] for the thermal stress analysis of FGM plates and shells, respectively. The temperature profile was defined in two ways: assumed as linear through the entire thickness direction or calculated by solving the 3D Fourier heat conduction equation. The 2D numerical models in [74]- [76] allowed the post-buckling analysis of FGM piezolectric shells in thermal environments when axial, lateral or hydrostatic loads were applied. Jabbari et al. [77] developed a semi-numerical higher order shear deformation theory for the thermal stress investigation

of FGM conical shells. The 2D FE model by Santos et al. [78] was based on the three-dimensional equations of motion. This model allowed the thermo-mechanical analysis of FGM cylindrical shells.

The new proposed exact 3D shell model is more general than those seen in the above literature survey. It allows the thermal stress analysis of one-layered and sandwich plates, cylinders and cylindrical and spherical shells embedding different FGM layers by using three different temperature profiles. When the temperature amplitudes are imposed at the external surfaces in steady-state conditions, the temperature profile through the thickness direction can be a priori assumed as linear, calculated using the 1D Fourier heat conduction equation or calculated by means of the 3D Fourier heat conduction problem. The present model is the extension to FGM structures of the previous authors' work [14] about the 3D exact thermal stress analysis of composite and sandwich plates and shells. The model is given in closed-form because of simply supported boundary conditions and harmonic forms for displacements and temperature. The 3D equilibrium equations in differential form are solved using the exponential matrix method and the layer-wise approach. This solution procedure was already applied by the first author in [79]- [88] in the case of pure mechanical free frequency and bending investigations of plates and shells embedding isotropic, orthotropic, composite and FGM layers. When a temperature profile is considered, the 3D differential equilibrium equations are not homogeneous any more and the exponential matrix method must be used for both general and particular solutions as seen in [89] and [90]. The 3D Fourier heat conduction equation is written in orthogonal mixed curvilinear coordinates using the suggestions proposed in [91]- [94]. Therefore, it is solved by means of the method proposed in [19] after the introduction of mathematical layers to obtain constant coefficients in place of variable coefficients. Variable coefficients are due to the presence of curvature terms for shells and through-the-thickness variable thermal and elastic coefficients for FGM layers. Section 2 proposes how to define, in a separated way, the temperature profile. Section 3 shows the 3D thermo-mechanical shell model and how to solve it via the exponential matrix method. Section 4 is about the results, presented as preliminary assessments to validate the model and as new benchmarks to introduce further comments and discussions. Section 5 is devoted to the main conclusions.

2 Through-the-thickness temperature evaluation

The thermo-mechanical exact 3D shell model proposed in Section 3 for FGM structures is based on a system of non-homogenous differential equations because of the known terms which are related to the thermal field. These terms are known because they are separately defined in the present section. When the temperature amplitudes are imposed at the external surfaces in steady-state conditions, the temperature profile through the thickness direction can be considered in three different ways: resolution of the 3D version of the Fourier heat conduction equation; resolution of the 1D version of the Fourier heat conduction equation; temperature profile imposed as linear through the entire thickness of the structure.

2.1 3D heat conduction problem

In the case of a spherical shell with constant radii of curvature in the two in-plane directions, an orthogonal mixed curvilinear reference system (α, β, z) can be defined. Figure 1 shows the employed reference system, the constant thickness h, the middle surface Ω_0, and the radii of curvature R_α and R_β along the α and β directions positioned on Ω_0. As proposed in [95], two parametric coefficients can be defined to consider the change of curvature with the transverse normal coordinate z or $\tilde{z}$ along the thickness direction:

$$H_\alpha = \left(1 + \frac{z}{R_\alpha}\right) = \left(1 + \frac{\tilde{z} - h/2}{R_\alpha}\right), \quad H_\beta = \left(1 + \frac{z}{R_\beta}\right) = \left(1 + \frac{\tilde{z} - h/2}{R_\beta}\right), \quad H_z = 1\,, \tag{1}$$

H_α and H_β depend on z (which goes from -$h/2$ to +$h/2$ with the zero positioned in the Ω_0 surface) or on $\tilde{z}$ (which varies from 0 to h and it is measured from the bottom surface). In the case of shells with constant radii of curvature, the coefficients H_α and H_β in Eq.(1) are a linear function of the thickness coordinate z or $\tilde{z}$. The parametric coefficient H_z is always equal to 1 because z or $\tilde{z}$ are always rectlinear coordinates. H_α or H_β equals 1 in the cases of cylinders and cylindrical panels because one of the two radii of curvature is ∞. $H_\alpha = H_\beta = 1$ in the case of plates because both the radii of curvature are infinite.

In the work [14], it was demonstrated how the 3D Fourier heat conduction equation can be written in orthogonal mixed curvilinear coordinates (α, β, z) by means of the considerations proposed in [92]. The final form is:

$$\frac{\kappa_1^k(z)}{H_\alpha^2(z)}\frac{\partial^2\theta}{\partial\alpha^2} + \frac{\kappa_2^k(z)}{H_\beta^2(z)}\frac{\partial^2\theta}{\partial\beta^2} + \kappa_3^k(z)\frac{\partial^2\theta}{\partial z^2} = 0\,. \tag{2}$$

Eq.(2) has not constant coefficients because conductivity coefficients $\kappa_1^k(z)$, $\kappa_2^k(z)$ and $\kappa_3^k(z)$ are functions of z in the case of Functionally Graded Material (FGM) layers and parametric coefficients $H_\alpha(z)$ and $H_\beta(z)$ are functions of z in the case of shell geometries. Eq.(2) can be rewritten as:

$$\kappa_1^{*k}(z)\frac{\partial^2\theta}{\partial\alpha^2} + \kappa_2^{*k}(z)\frac{\partial^2\theta}{\partial\beta^2} + \kappa_3^{*k}(z)\frac{\partial^2\theta}{\partial z^2} = 0\,, \tag{3}$$

where the variable coefficients are defined as:

$$\kappa_1^{*k}(z) = \frac{\kappa_1^k(z)}{H_\alpha^2(z)}, \quad \kappa_2^{*k}(z) = \frac{\kappa_2^k(z)}{H_\beta^2(z)}, \quad \kappa_3^{*k}(z) = \kappa_3^k(z)\,. \tag{4}$$

In each k physical layer, coefficients $\kappa_1^{*k}(z)$, $\kappa_2^{*k}(z)$ and $\kappa_3^{*k}(z)$ are functions of z because of functionally graded material and/or curvature effects. In order to obtain Eq.(3) with constant coefficients, a certain number M of mathematical layers is introduced to calculate, in several points through the thickness direction, the appropriate values for the conductivity coefficients κ_1, κ_2 and κ_3 and for the parametric coefficients H_α and H_β. The index k of the physical layers goes from 1 to the total number of physical layers N_L. A new index j is introduced for the mathematical layers which goes from 1 to M (total number of mathematical layers used to opportunely divide the entire thickness of the structure). The 3D Fourier heat conduction equation with constant coefficients for a j mathematical layer is:

$$\kappa_1^{*j}\frac{\partial^2\theta}{\partial\alpha^2} + \kappa_2^{*j}\frac{\partial^2\theta}{\partial\beta^2} + \kappa_3^{*j}\frac{\partial^2\theta}{\partial z^2} = 0\,. \tag{5}$$

Eq.(5) can be now exactly solved in the case of simply supported boundary conditions, bi-sinusoidal form for the temperature θ^j in the in-plane directions and temperature amplitudes Θ^j imposed at the external surfaces in steady-state conditions. The method is that proposed in [19] and already successfully applied in the companion paper [14] about classical composite and sandwich shells.

The harmonic form for the temperature field is:

$$\theta^j(\alpha, \beta, z) = \Theta^j(z) sin(\bar{\alpha}\alpha) sin(\bar{\beta}\beta)\,, \tag{6}$$

where $\Theta^j(z)$ is the temperature amplitude, and the two coefficients $\bar{\alpha}$ and $\bar{\beta}$ are defined as $\bar{\alpha} = \frac{m\pi}{a}$ and $\bar{\beta} = \frac{n\pi}{b}$. a and b are the shell dimensions; m and n are the half-wave numbers in α and β directions, respectively. The temperature amplitude is imposed at the external surfaces as Θ_b^1 (value at the bottom (b) of the first mathematical layer 1) and Θ_t^M (value at the top (t) of the last mathematical layer M). Eq.(5) is satisfied by the introduction of the harmonic form for the temperature $\theta^j(\alpha, \beta, z)$ proposed in Eq.(6). In this case, the dependence of the amplitude $\Theta^j(z)$ from the z coordinate can be expressed as:

$$\Theta^j(z) = \Theta_0^j \exp(s^j z)\,, \tag{7}$$

Θ_0^j and s^j must be calculated in each j mathematical layer. s^j is calculated via the substitution of Eq. (6) in Eq.(5) remembering the assumption made in Eq.(7):

$$s_{1,2}^j = \pm\sqrt{\frac{\kappa_1^{*j}\bar{\alpha}^2 + \kappa_2^{*j}\bar{\beta}^2}{\kappa_3^{*j}}}\,, \tag{8}$$

s_1^j is the chosen solution. Therefore, Eq.(7) can be expressed as:

$$\Theta^j(z) = \Theta_{01}^j \exp(s_1^j z) + \Theta_{02}^j \exp(s_1^j z)\,, \tag{9}$$

$$\Theta^j(z) = S_1^j cosh(s_1^j z) + S_2^j sinh(s_1^j z)\,. \tag{10}$$

Eq.(9) or Eq.(10) has two parameters which must be calculated for each j mathematical layer. For example, Eq.(10) has $2 \times M$ coefficients (S_1^j and S_2^j) which must be determined. s_1^j for each j layer is obtained using Eq.(8) with the + as algebraic sign. Unknown coefficients can be calculated by means of two continuity conditions at each interface between two adjacent layers:

$$\Theta_b^{(j+1)} = \Theta_t^j\,, \tag{11}$$

$$\kappa_3^{*j+1}\Theta_{,z_b}^{(j+1)} = \kappa_3^{*j}\Theta_{,z_t}^j\,. \tag{12}$$

Eq.(11) means that the temperature at the top (t) of the generic j layer must be equal to the temperature at the bottom (b) of the $(j+1)$ layer. Eq.(12) allows the equivalence of the heath flux q_3 in the thickness direction z by means of its evaluation at the bottom (b) of the $(j+1)$ layer and at the top (t) of the j layer. Combining Eqs.(11), (12) and (10), a compact matrix form, which links parameters S_1 and S_2 at the j layer with parameters S_1 and S_2 at the $(j+1)$ layer, is obtained:

$$\begin{bmatrix} S_1 \\ S_2 \end{bmatrix}^{j+1} = \begin{bmatrix} V_{\Theta 1}^{j+1,j} & V_{\Theta 2}^{j+1,j} \\ V_{\Theta 3}^{j+1,j} & V_{\Theta 4}^{j+1,j} \end{bmatrix} \begin{bmatrix} S_1 \\ S_2 \end{bmatrix}^{j}\,. \tag{13}$$

In this way, a total number of $2 \times (M-1)$ conditions are imposed for all the $(M-1)$ interfaces present in the structure. Calling the transfer matrix of Eq.(13) as $\boldsymbol{V}_{\Theta}^{(j+1,j)}$, coefficients at the top layer ($j = M$) and those at the bottom layer ($j = 1$) can be linked using recursively Eq.(13):

$$\begin{bmatrix} S_1 \\ S_2 \end{bmatrix}^{M} = \boldsymbol{V}_{\Theta}^{(M,M-1)}\boldsymbol{V}_{\Theta}^{(M-1,M-2)}.....\boldsymbol{V}_{\Theta}^{(3,2)}\boldsymbol{V}_{\Theta}^{(2,1)} \begin{bmatrix} S_1 \\ S_2 \end{bmatrix}^{1} = \boldsymbol{V}_{\Theta}^{(M,1)} \begin{bmatrix} S_1 \\ S_2 \end{bmatrix}^{1}\,. \tag{14}$$

The problem proposed in Eq.(14) can be solved adding the temperature conditions at the bottom and at the top of the entire shell (they are known). Therefore, the 2 values missed in the $2 \times (M-1)$ conditions already imposed in Eqs.(13) and (14) are obtained. In this way, all the $2 \times M$ coefficients (S_1^j and S_2^j for all the M mathematical layers) can be calculated. Once the coefficients in the external layers have been defined, the other coefficients can be easily calculated and the temperature profile can be defined.

When the 3D exact thermo-mechanical shell model developed in Section 3 will use this temperature profile, calculated via the 3D heat conduction problem, it will be called as 3D(θ_c,3D) model.

2.2 1D heat conduction problem

If we consider the temperature field in the bi-sinusoidal form as proposed in Eq.(6), the three heat fluxes in α, β and z directions can be calculated as derivatives of the temperature made with respect

to α, β and z coordinates, respectively:

$$q_1^j = -\kappa_1^{*j}\bar{\alpha}\Theta^j(z)cos(\bar{\alpha}\alpha)sin(\bar{\beta}\beta)\,, \tag{15}$$

$$q_2^j = -\kappa_2^{*j}\bar{\beta}\Theta^j(z)sin(\bar{\alpha}\alpha)cos(\bar{\beta}\beta)\,, \tag{16}$$

$$q_3^j = -\kappa_3^{*j}\Theta^j_{,z}(z)sin(\bar{\alpha}\alpha)sin(\bar{\beta}\beta)\,. \tag{17}$$

In the case of very thin structures (high values of thickness ratio), the 3D problem can be simplified in a 1D problem where the heat fluxes q_1^j and q_2^j can be discarded. Therefore, the heat flux q_3 remains constant for the entire thickness of the structure and it can be defined as:

$$q_3 = -\frac{1}{R_{z_{eq}}}(\Theta_t - \Theta_b) = const.\,, \tag{18}$$

where Θ_t and Θ_b are the imposed sovra-temperature amplitudes, in steady-sate conditions, at the top and bottom external surfaces, respectively. The constant heat flux q_3 through the entire thickness of the structure can be calculated using the equivalent thermal resistance $R_{z_{eq}}$ by means of the following relation:

$$R_{z_{eq}} = \sum_{j=1}^{M}\frac{h^j}{\kappa_3^{*j}}\,, \tag{19}$$

where h^j is the thickness of each j mathematical layer, κ_3^{*j} is the conductivity coefficient calculated as a constant term in each j mathematical layer employed to discretize the FGM layers. The summation goes from 1 (first mathematical layer at the bottom) to M (last mathematical layer at the top).

After the definition of the global and constant heat flux q_3, the heat flux in each j mathematical layer can be defined as:

$$q_3^j = -\kappa_3^{*j}\frac{\partial\Theta^j}{\partial z} = -\frac{\kappa_3^{*j}}{h^j}(\Theta_t^j - \Theta_b^j)\,, \tag{20}$$

where the temperature gradient in each j mathematical layer is calculated by means of the thickness h^j of each j layer and the temperature amplitudes Θ_t^j and Θ_b^j defined at the top and bottom of each j layer, respectively. Eq.(20) can be used to write that the heat flux in the j layer is equal to the heat flux in the $j+1$ layer, and then they are equal to the global heat flux q_3:

$$q_3^j = -\kappa_3^{*j}\frac{(\Theta_t^j - \Theta_b^j)}{h^j} = q_3^{j+1} = -\kappa_3^{*j+1}\frac{(\Theta_t^{j+1} - \Theta_b^{j+1})}{h^{j+1}} = q_3 = const.\,. \tag{21}$$

The heat flux q_3, the thickness h^j of each j layer, the temperature values at the external surfaces of the entire structure Θ_t and Θ_b (imposed values) are known terms in Eq.(21). Therefore, this equation can be used to calculate all the temperature amplitudes at each interface between two adjacent j layers. In this way, the temperature profile has been defined in the entire thickness of the structure. When the value of κ_3^{*j} changes, moving from the j layer to the $j+1$ layer, the slope of the temperature profile also changes but it remains linear in each j layer because the 3D effect has been discarded. Therefore, the thickness layer effect, which gives temperature profiles different from the linear ones, is not considered in each j layer. The thickness layer effect (temperature profile not linear in the considered thick j layer) is only captured by the 3D Fourier heat conduction equation seen in the previous subsection. However, a complicated temperature profile through the entire thickness of the FGM structure can be reconstructed with a good approximation using these local linear evaluations for each j layer.

When the 3D exact thermo-mechanical shell model developed in Section 3 will use this temperature profile, calculated via the 1D heat conduction problem, it will be called as 3D(θ_c,1D) model.

2.3 A priori linear assumed temperature profile

A third possibility to define the temperature profile is to consider it as a linear evaluation from the known and imposed top temperature amplitude Θ_t to the known and imposed bottom temperature amplitude Θ_b. In this way, both thickness layer and material layer effects are discarded and the temperature profile is always linear through the entire thickness even if the structure is thick and not homogeneous. This simplified hypothesis is very common in the literature and it gives important errors even if the mechanical model is appropriate. This profile is valid only for thin and homogeneous one-layered plates and shells.

When the 3D exact thermo-mechanical shell model developed in Section 3 will use this imposed linear temperature profile, it will be called as 3D(θ_a) model.

3 3D shell model in closed form

In the case of spherical shells embedding N_L physical layers with constant radii of curvature R_α and R_β, the 3D differential equilibrium equations for a generic k physical FGM layer can be written as:

$$H_\beta(z)\frac{\partial \sigma^k_{\alpha\alpha}}{\partial\alpha} + H_\alpha(z)\frac{\partial \sigma^k_{\alpha\beta}}{\partial\beta} + H_\alpha(z)H_\beta(z)\frac{\partial \sigma^k_{\alpha z}}{\partial z} + \left(\frac{2H_\beta(z)}{R_\alpha} + \frac{H_\alpha(z)}{R_\beta}\right)\sigma^k_{\alpha z} = 0, \tag{22}$$

$$H_\beta(z)\frac{\partial \sigma^k_{\alpha\beta}}{\partial\alpha} + H_\alpha(z)\frac{\partial \sigma^k_{\beta\beta}}{\partial\beta} + H_\alpha(z)H_\beta(z)\frac{\partial \sigma^k_{\beta z}}{\partial z} + \left(\frac{2H_\alpha(z)}{R_\beta} + \frac{H_\beta(z)}{R_\alpha}\right)\sigma^k_{\beta z} = 0, \tag{23}$$

$$H_\beta(z)\frac{\partial \sigma^k_{\alpha z}}{\partial\alpha} + H_\alpha(z)\frac{\partial \sigma^k_{\beta z}}{\partial\beta} + H_\alpha(z)H_\beta(z)\frac{\partial \sigma^k_{zz}}{\partial z} - \frac{H_\beta(z)}{R_\alpha}\sigma^k_{\alpha\alpha} - \frac{H_\alpha(z)}{R_\beta}\sigma^k_{\beta\beta} + \left(\frac{H_\beta(z)}{R_\alpha} + \frac{H_\alpha(z)}{R_\beta}\right)\sigma^k_{zz} = 0\,. \tag{24}$$

Parametric coefficients are not constant because they depend on the thickness coordinate z. Eqs.(22)-(24) are valid for spherical shell geometry with constant radii of curvature (see Figure 1), and they degenerate in equations for cylinders and cylindrical panels (when one of the two radii of curvature is ∞) and in equations for plates (when both the radii of curvature are ∞). Possible examples are the benchmarks proposed in Figure 2.

The geometrical relations in an orthogonal mixed curvilinear reference system (α, β, z) have the following form in the case of a k FGM layer. The sovra-temperature field $\theta\,(\alpha,\,\beta,\,z)$ is defined with respect to a reference temperature T_0 as $\theta = T - T_0$:

$$\epsilon^k_{\alpha\alpha} = \epsilon^k_{\alpha\alpha m} - \epsilon^k_{\alpha\alpha\theta} = \frac{1}{H_\alpha(z)}\frac{\partial u^k}{\partial\alpha} + \frac{w^k}{H_\alpha(z)R_\alpha} - \mu^k(z)\theta^k\,, \tag{25}$$

$$\epsilon^k_{\beta\beta} = \epsilon^k_{\beta\beta m} - \epsilon^k_{\beta\beta\theta} = \frac{1}{H_\beta(z)}\frac{\partial v^k}{\partial\beta} + \frac{w^k}{H_\beta(z)R_\beta} - \mu^k(z)\theta^k\,, \tag{26}$$

$$\epsilon^k_{zz} = \epsilon^k_{zzm} - \epsilon^k_{zz\theta} = \frac{\partial w^k}{\partial z} - \mu^k(z)\theta^k\,, \tag{27}$$

$$\gamma^k_{\beta z} = \gamma^k_{\beta z m} = \frac{1}{H_\beta(z)}\frac{\partial w^k}{\partial\beta} + \frac{\partial v^k}{\partial z} - \frac{v^k}{H_\beta(z)R_\beta}\,, \tag{28}$$

$$\gamma^k_{\alpha z} = \gamma^k_{\alpha z m} = \frac{1}{H_\alpha(z)}\frac{\partial w^k}{\partial\alpha} + \frac{\partial u^k}{\partial z} - \frac{u^k}{H_\alpha(z)R_\alpha}\,, \tag{29}$$

$$\gamma^k_{\alpha\beta} = \gamma^k_{\alpha\beta m} = \frac{1}{H_\alpha(z)}\frac{\partial v^k}{\partial\alpha} + \frac{1}{H_\beta(z)}\frac{\partial u^k}{\partial\beta}\,, \tag{30}$$

in the case of a k FGM layer, which is isotropic in the plane directions and not homogeneous through the thickness direction, the thermal expansion coefficients depend on the thickness coordinate z: $\mu^k_\alpha(z) = \mu^k_\beta(z) = \mu^k_z(z) = \mu^k(z)$. In this case, the structural reference system (α, β, z) is coincident with the material reference system (1, 2, 3). ($\epsilon^k_{\alpha\alpha}$, $\epsilon^k_{\beta\beta}$, ϵ^k_{zz}, $\gamma^k_{\beta z}$, $\gamma^k_{\alpha z}$, $\gamma^k_{\alpha\beta}$) are the six strain components for the k FGM layer and they can be seen as the algebraic summation of mechanical strains (subscript m) and thermal strains (subscript θ). They are functions of the three displacement components u^k, v^k and w^k in α, β, z direction, respectively, and of the temperature θ^k by means of the thermal expansion coefficients $\mu^k(z)$.

The constitutive equations have variable elastic and thermal coefficients in the case of a k FGM layer:

$$\boldsymbol{\sigma}^k = \boldsymbol{C}^k(z)\boldsymbol{\epsilon}^k = \boldsymbol{C}^k(z)[\boldsymbol{\epsilon}^k_m - \boldsymbol{\epsilon}^k_\theta]\,, \tag{31}$$

where the stress vector $\boldsymbol{\sigma}^k = [\sigma^k_{\alpha\alpha}\,\sigma^k_{\beta\beta}\,\sigma^k_{zz}\,\sigma^k_{\beta z}\,\sigma^k_{\alpha z}\,\sigma^k_{\alpha\beta}]^T$ has dimension 6×1, the elastic coefficient matrix $\boldsymbol{C}^k(z)$ has dimension 6×6 and the strains have been defined in Eqs.(25)-(30). T means the transpose of a vector. The elastic coefficient matrix for a k FGM isotropic layer is:

$$\boldsymbol{C}^k(z) = \begin{bmatrix} C^k_{11}(z) & C^k_{12}(z) & C^k_{13}(z) & 0 & 0 & 0 \\ C^k_{12}(z) & C^k_{22}(z) & C^k_{23}(z) & 0 & 0 & 0 \\ C^k_{13}(z) & C^k_{23}(z) & C^k_{33}(z) & 0 & 0 & 0 \\ 0 & 0 & 0 & C^k_{44}(z) & 0 & 0 \\ 0 & 0 & 0 & 0 & C^k_{55}(z) & 0 \\ 0 & 0 & 0 & 0 & 0 & C^k_{66}(z) \end{bmatrix}. \tag{32}$$

After the opportune substitutions, the explicit form of Eq.(31) is:

$$\sigma^k_{\alpha\alpha} = \frac{C^k_{11}(z)}{H_\alpha(z)}u^k_{,\alpha} + \frac{C^k_{11}(z)}{H_\alpha(z)R_\alpha}w^k + \frac{C^k_{12}(z)}{H_\beta(z)}v^k_{,\beta} + \frac{C^k_{12}(z)}{H_\beta(z)R_\beta}w^k + C^k_{13}(z)w^k_{,z} - \lambda^k_1(z)\theta^k\,, \tag{33}$$

$$\sigma^k_{\beta\beta} = \frac{C^k_{12}(z)}{H_\alpha(z)}u^k_{,\alpha} + \frac{C^k_{12}(z)}{H_\alpha(z)R_\alpha}w^k + \frac{C^k_{22}(z)}{H_\beta(z)}v^k_{,\beta} + \frac{C^k_{22}(z)}{H_\beta(z)R_\beta}w^k + C^k_{23}(z)w^k_{,z} - \lambda^k_2(z)\theta^k\,, \tag{34}$$

$$\sigma^k_{zz} = \frac{C^k_{13}(z)}{H_\alpha(z)}u^k_{,\alpha} + \frac{C^k_{13}(z)}{H_\alpha(z)R_\alpha}w^k + \frac{C^k_{23}(z)}{H_\beta(z)}v^k_{,\beta} + \frac{C^k_{23}(z)}{H_\beta(z)R_\beta}w^k + C^k_{33}(z)w^k_{,z} - \lambda^k_3(z)\theta^k\,, \tag{35}$$

$$\sigma^k_{\beta z} = \frac{C^k_{44}(z)}{H_\beta(z)}w^k_{,\beta} + C^k_{44}(z)v^k_{,z} - \frac{C^k_{44}(z)}{H_\beta(z)R_\beta}v^k\,, \tag{36}$$

$$\sigma^k_{\alpha z} = \frac{C^k_{55}(z)}{H_\alpha(z)}w^k_{,\alpha} + C^k_{55}(z)u^k_{,z} - \frac{C^k_{55}(z)}{H_\alpha(z)R_\alpha}u^k\,, \tag{37}$$

$$\sigma^k_{\alpha\beta} = \frac{C^k_{66}(z)}{H_\alpha(z)}v^k_{,\alpha} + \frac{C^k_{66}(z)}{H_\beta(z)}u^k_{,\beta}\,, \tag{38}$$

where subscripts $(,\alpha)$, $(,\beta)$ and $(,z)$ indicate the related partial derivatives $(\frac{\partial}{\partial\alpha})$, $(\frac{\partial}{\partial\beta})$ and $(\frac{\partial}{\partial z})$, respectively. The thermo-mechanical coupling coefficients $\lambda^k_1(z)$, $\lambda^k_2(z)$ and $\lambda^k_3(z)$ used in Eqs.(33)-(38) are calculated as:

$$\lambda^k_\alpha(z) = C^k_{11}(z)\mu^k(z) + C^k_{12}(z)\mu^k(z) + C^k_{13}(z)\mu^k(z)\,, \tag{39}$$

$$\lambda^k_\beta(z) = C^k_{12}(z)\mu^k(z) + C^k_{22}(z)\mu^k(z) + C^k_{23}(z)\mu^k(z)\,, \tag{40}$$

$$\lambda^k_z(z) = C^k_{13}(z)\mu^k(z) + C^k_{23}(z)\mu^k(z) + C^k_{33}(z)\mu^k(z)\,. \tag{41}$$

One of the main hypotheses to obtain the closed form solution of the equilibrium equations (22)-(24) is the harmonic form for displacements and temperature (see Eq.(6)) which means simply supported

sides. The harmonic form for displacements is:

$$u^k(\alpha,\beta,z) = U^k(z)cos(\bar{\alpha}\alpha)sin(\bar{\beta}\beta)\ , \tag{42}$$

$$v^k(\alpha,\beta,z) = V^k(z)sin(\bar{\alpha}\alpha)cos(\bar{\beta}\beta)\ , \tag{43}$$

$$w^k(\alpha,\beta,z) = W^k(z)sin(\bar{\alpha}\alpha)sin(\bar{\beta}\beta)\ , \tag{44}$$

the two coefficients $\bar{\alpha}$ and $\bar{\beta}$ have the same meaning already seen in Eq.(6) for the temperature. $U^k(z)$, $V^k(z)$ and $W^k(z)$ are the displacement amplitudes. Substituting the harmonic forms for the displacements (Eqs.(42)-(44)) and for the temperature (Eq.(6)) into the constitutive equations (33)-(38) and into the equilibrium equations (22)-(24), it is possible to obtain a system of three differential equations in terms of amplitudes for displacements and temperature and their related derivatives made with respect to z. The derivatives in α and β directions have been exactly calculated using the harmonic forms and they are known algebraic terms. Therefore, the system is now made of three differential equations of second order in z. These equations have not constant coefficients because of H_α and H_β (which are functions of z for shells) and because of elastic and thermal coefficients (which depend on z in the case of a k FGM layer). This system can be written in compact form using coefficients $A^k_s(z)$ (with s from 1 to 19) and coefficients $J^k_r(z)$ (with r from 1 to 4):

$$A^k_1(z)U^k + A^k_2(z)V^k + A^k_3(z)W^k + A^k_4(z)U^k_{,z} + A^k_5(z)W^k_{,z} + A^k_6(z)U^k_{,zz} + J^k_1(z)\Theta^k = 0\ , \tag{45}$$

$$A^k_7(z)U^k + A^k_8(z)V^k + A^k_9(z)W^k + A^k_{10}(z)V^k_{,z} + A^k_{11}(z)W^k_{,z} + A^k_{12}(z)V^k_{,zz} + J^k_2(z)\Theta^k = 0\ , \tag{46}$$

$$A^k_{13}(z)U^k + A^k_{14}(z)V^k + A^k_{15}(z)W^k + A^k_{16}(z)U^k_{,z} + A^k_{17}(z)V^k_{,z} + A^k_{18}(z)W^k_{,z} + A^k_{19}(z)W^k_{,zz} + \tag{47}$$
$$J^k_3(z)\Theta^k_{,z} + J^k_4(z)\Theta^k = 0\ .$$

Coefficients $A^k_s(z)$ and $J^k_r(z)$ depend on z because of the parametric terms $H_\alpha(z)$ and $H_\beta(z)$ and variable material properties of the FGM layers. For this reason, each k physical layer is divided in a certain number of mathematical layers. Therefore, a new index j is defined for the global mathematical layers and it goes from 1 to the total number of mathematical layers M. In the middle of each j mathematical layer, the coefficients H_α and H_β and FGM elastic and thermal properties are exactly calculated. Eqs.(45)-(47) can be now rewritten as constant coefficient equations:

$$A^j_1U^j + A^j_2V^j + A^j_3W^j + A^j_4U^j_{,z} + A^j_5W^j_{,z} + A^j_6U^j_{,zz} + J^j_1\Theta^j = 0\ , \tag{48}$$

$$A^j_7U^j + A^j_8V^j + A^j_9W^j + A^j_{10}V^j_{,z} + A^j_{11}W^j_{,z} + A^j_{12}V^j_{,zz} + J^j_2\Theta^j = 0\ , \tag{49}$$

$$A^j_{13}U^j + A^j_{14}V^j + A^j_{15}W^j + A^j_{16}U^j_{,z} + A^j_{17}V^j_{,z} + A^j_{18}W^j_{,z} + A^j_{19}W^j_{,zz} + J^j_3\Theta^j_{,z} + J^j_4\Theta^j = 0\ . \tag{50}$$

The temperature profiles across z can be externally defined as seen in Section 2. Therefore, Eqs.(48)-(50) become a system of second order differential equations in the displacement amplitudes U^j, V^j, W^j and their derivatives in z. As discussed in [96] and [97], the system can be modified in a first order one by reducing the order of derivatives in z via the redoubling of the number of variables for each j layer (from 3 (U^j, V^j, W^j) to 6 (U^j, V^j, W^j, $U^{j'}$, $V^{j'}$, $W^{j'}$)). Terms Θ and Θ' are known terms as defined in Section 2. Superscript $'$ is used to indicate the derivatives performed with respect to z (also

indicated as $\frac{\partial}{\partial z}$):

$$\begin{bmatrix} A_6^j & 0 & 0 & 0 & 0 & 0 \\ 0 & A_{12}^j & 0 & 0 & 0 & 0 \\ 0 & 0 & A_{19}^j & 0 & 0 & 0 \\ 0 & 0 & 0 & 0 & 0 & 0 \\ 0 & 0 & 0 & 0 & 0 & 0 \\ 0 & 0 & 0 & 0 & 0 & 0 \end{bmatrix} \begin{bmatrix} U^j \\ V^j \\ W^j \\ U^{j'} \\ V^{j'} \\ W^{j'} \end{bmatrix}' =$$

$$\begin{bmatrix} 0 & 0 & 0 & A_6^j & 0 & 0 \\ 0 & 0 & 0 & 0 & A_{12}^j & 0 \\ 0 & 0 & 0 & 0 & 0 & A_{19}^j \\ -A_1^j & -A_2^j & -A_3^j & -A_4^j & 0 & -A_5^j \\ -A_7^j & -A_8^j & -A_9^j & 0 & -A_{10}^j & -A_{11}^j \\ -A_{13}^j & -A_{14}^j & -A_{15}^j & -A_{16}^j & -A_{17}^j & -A_{18}^j \end{bmatrix} \begin{bmatrix} U^j \\ V^j \\ W^j \\ U^{j'} \\ V^{j'} \\ W^{j'} \end{bmatrix} + \begin{bmatrix} 0 & 0 & 0 & 0 & 0 & 0 \\ 0 & 0 & 0 & 0 & 0 & 0 \\ 0 & 0 & 0 & 0 & 0 & 0 \\ -J_1^j & 0 & 0 & 0 & 0 & 0 \\ -J_2^j & 0 & 0 & 0 & 0 & 0 \\ -J_4^j & -J_3^j & 0 & 0 & 0 & 0 \end{bmatrix} \begin{bmatrix} \Theta^j \\ \Theta^{j'} \\ 0 \\ 0 \\ 0 \\ 0 \end{bmatrix}, \quad (51)$$

A compact form of Eq. (51) is:

$$\boldsymbol{D}^j \boldsymbol{U}^{j'} = \boldsymbol{A}^j \boldsymbol{U}^j + \boldsymbol{J}^j \boldsymbol{\Theta}^j \,, \quad (52)$$

the vectors are defined as $\boldsymbol{U}^j = [U^j \; V^j \; W^j \; U^{j'} \; V^{j'} \; W^{j'}]^T$, $\boldsymbol{U}^{j'} = \frac{\partial \boldsymbol{U}^j}{\partial z}$ and $\boldsymbol{\Theta}^j = [\Theta^j \; \Theta^{j'} \; 0 \; 0 \; 0 \; 0]^T$. Eq. (52) can be rewritten as:

$$\boldsymbol{U}^{j'} = \boldsymbol{D}^{j^{-1}} \boldsymbol{A}^j \boldsymbol{U}^j + \boldsymbol{D}^{j^{-1}} \boldsymbol{J}^j \boldsymbol{\Theta}^j \,, \quad (53)$$

$$\boldsymbol{U}^{j'} = \boldsymbol{A}^{*j} \boldsymbol{U}^j + \boldsymbol{J}^{*j} \boldsymbol{\Theta}^j \,, \quad (54)$$

indicating $\boldsymbol{A}^{*j} = \boldsymbol{D}^{j^{-1}} \boldsymbol{A}^j$ and $\boldsymbol{J}^{*j} = \boldsymbol{D}^{j^{-1}} \boldsymbol{J}^j$. The temperature amplitude can be assumed in each j mathematical layer as:

$$\Theta^j(\tilde{z}^j) = a_\Theta^j \tilde{z}^j + b_\Theta^j \,, \quad (55)$$

a_Θ^j and b_Θ^j are constant in each j layer. $\tilde{z}^j$ is the local thickness coordinate as defined in Figure 1 (from 0 at the bottom of the generic j layer to h^j at the top, where h^j is the thickness of the j mathematical layer). Coefficients a_Θ^j and b_Θ^j are calculated in each j layer independently by the method used to define the temperature profile (see Section 2). Eq.(54) is a system of first order differential equations in $\tilde{z}$ or z; these equations are not homogeneous because the thermal term $\boldsymbol{J}^{*j} \boldsymbol{\Theta}^j$ is a known function of $\tilde{z}^j$ or z^j defined in each point through the thickness.

The known term in Eq.(54) can be explicitly calculated using the known temperature values defined in Section 2:

$$\boldsymbol{\Theta}^{*j} = \boldsymbol{J}^{*j} \boldsymbol{\Theta}^j = \begin{bmatrix} 0 & 0 & 0 & 0 & 0 & 0 \\ 0 & 0 & 0 & 0 & 0 & 0 \\ 0 & 0 & 0 & 0 & 0 & 0 \\ -J_1^{*j} & 0 & 0 & 0 & 0 & 0 \\ -J_2^{*j} & 0 & 0 & 0 & 0 & 0 \\ -J_4^{*j} & -J_3^{*j} & 0 & 0 & 0 & 0 \end{bmatrix} \begin{bmatrix} a_\Theta^j \tilde{z}^j + b_\Theta^j \\ a_\Theta^j \\ 0 \\ 0 \\ 0 \\ 0 \end{bmatrix} = \begin{bmatrix} 0 \\ 0 \\ 0 \\ -J_1^{*j}(a_\Theta^j \tilde{z}^j + b_\Theta^j) \\ -J_2^{*j}(a_\Theta^j \tilde{z}^j + b_\Theta^j) \\ -J_4^{*j}(a_\Theta^j \tilde{z}^j + b_\Theta^j) - J_3^{*j} a_\Theta^j \end{bmatrix}. \quad (56)$$

In this way, the compact form of Eq.(54) is:

$$\boldsymbol{U}^{j'} = \boldsymbol{A}^{*j} \boldsymbol{U}^j + \boldsymbol{\Theta}^{*j} \,, \quad (57)$$

where $\boldsymbol{\Theta}^{*j}$ contains functions of $\tilde{z}^j$. The Eq.(57) can be solved by means of:

$$\boldsymbol{U}^j(\tilde{z}^j) = \mathrm{e}^{(\boldsymbol{A}^{*j} \tilde{z}^j)} \boldsymbol{U}^j(0) + \int_0^{\tilde{z}^j} \mathrm{e}^{(\boldsymbol{A}^{*j}(\tilde{z}^j - s))} \boldsymbol{\Theta}^{*j}(s) ds \,. \quad (58)$$

Eq.(58) can be used to calculate the displacement vector at the top of the j layer when the terms $\boldsymbol{A}^{**^j} = \mathrm{e}^{(\boldsymbol{A}^{*^j} h^j)}$ and $\boldsymbol{J}^{**^j} = \int_0^{h^j} \mathrm{e}^{(\boldsymbol{A}^{*^j}(h^j - s))} \boldsymbol{\Theta}^{*^j}(s) ds$ have been evaluated for each j layer with thickness h^j. The exponential matrix can be expanded and evaluated in each j layer with thickness h^j using the known procedure seen in [14], [96] and [97]:

$$\boldsymbol{A}^{**^j} = \mathrm{e}^{(\boldsymbol{A}^{*^j} h^j)} = \boldsymbol{I} + \boldsymbol{A}^{*^j} h^j + \frac{\boldsymbol{A}^{*^j\,2}}{2!} h^{j\,2} + \frac{\boldsymbol{A}^{*^j\,3}}{3!} h^{j\,3} + \cdots + \frac{\boldsymbol{A}^{*^j\,N}}{N!} h^{j\,N} \,, \tag{59}$$

where $\boldsymbol{I}$ is the identity matrix with dimension 6×6. The integral in Eq.(58) can be calculated for each j layer with thickness h^j by expanding the exponential matrix with the same methodology and the same order N seen in Eq.(59):

$$\begin{aligned} \boldsymbol{J}^{**^j} = \int_0^{h^j} \mathrm{e}^{(\boldsymbol{A}^{*^j}(h^j - s))} \boldsymbol{\Theta}^{*^j}(s) ds = \int_0^{h^j} \Big(\boldsymbol{I} + \boldsymbol{A}^{*^j}(h^j - s) + \frac{\boldsymbol{A}^{*^j\,2}}{2!}(h^j - s)^2 + \frac{\boldsymbol{A}^{*^j\,3}}{3!}(h^j - s)^3 + \\ \cdots + \frac{\boldsymbol{A}^{*^j\,N}}{N!}(h^j - s)^N \Big) \boldsymbol{\Theta}^{*^j}(s) ds \,. \end{aligned} \tag{60}$$

In this way, Eq.(58) can be defined, by means of Eqs.(59) and (60), as:

$$\boldsymbol{U}^j(h^j) = \boldsymbol{A}^{**^j} \boldsymbol{U}^j(0) + \boldsymbol{J}^{**^j} \,, \tag{61}$$

this equation can be rewritten as:

$$\boldsymbol{U}_t^j = \boldsymbol{A}^{**^j} \boldsymbol{U}_b^j + \boldsymbol{J}^{**^j} \,, \tag{62}$$

where $\boldsymbol{U}^j(h^j)$ is $\boldsymbol{U}_t^j$ and $\boldsymbol{U}^j(0)$ is $\boldsymbol{U}_b^j$. t and b are the top and the bottom of the j layer, respectively.

The top and bottom displacements (and the relative derivatives in $\tilde{z}$) for a mathematical j layer can be linked using Eq.(62). In this way, a set of interlaminar conditions must be imposed. The continuity of the displacements at each interface is defined as:

$$u_b^j = u_t^{j-1} \,, \;\; v_b^j = v_t^{j-1} \,, \;\; w_b^j = w_t^{j-1} \,. \tag{63}$$

The conditions given by Eqs.(63) can be also written in terms of displacement amplitudes U^j, V^j and W^j. The continuity of transverse shear/normal stresses is:

$$\sigma_{zz_b}^j = \sigma_{zz_t}^{j-1} \,, \;\; \sigma_{\alpha z_b}^j = \sigma_{\alpha z_t}^{j-1} \,, \;\; \sigma_{\beta z_b}^j = \sigma_{\beta z_t}^{j-1} \,. \tag{64}$$

In Eqs.(63) and (64), the bottom (b) values for the generic j layer and the top (t) values of the $(j-1)$ layer must be equal. The constitutive equations (33)-(38) and the harmonic form for the displacements and temperature allow a displacement form of Eqs.(63) and (64) to be obtained. The method was already illustrated in [79]- [83]. In addition, in the present paper, the continuity equation for the transverse normal stress σ_{zz} has an additional thermal term which is given using the coefficient T_{11}. The compact displacement form of Eqs.(63) and (64), by means of two transfer matrices $\boldsymbol{T}$, is:

$$\begin{bmatrix} U \\ V \\ W \\ U' \\ V' \\ W' \end{bmatrix}^j_b = \begin{bmatrix} 1 & 0 & 0 & 0 & 0 & 0 \\ 0 & 1 & 0 & 0 & 0 & 0 \\ 0 & 0 & 1 & 0 & 0 & 0 \\ T_1 & 0 & T_2 & T_3 & 0 & 0 \\ 0 & T_4 & T_5 & 0 & T_6 & 0 \\ T_7 & T_8 & T_9 & 0 & 0 & T_{10} \end{bmatrix}^{j-1,j} \begin{bmatrix} U \\ V \\ W \\ U' \\ V' \\ W' \end{bmatrix}^{j-1}_t + \begin{bmatrix} 0 & 0 & 0 & 0 & 0 & 0 \\ 0 & 0 & 0 & 0 & 0 & 0 \\ 0 & 0 & 0 & 0 & 0 & 0 \\ 0 & 0 & 0 & 0 & 0 & 0 \\ 0 & 0 & 0 & 0 & 0 & 0 \\ T_{11} & 0 & 0 & 0 & 0 & 0 \end{bmatrix}^{j-1,j} \begin{bmatrix} \Theta \\ \Theta' \\ 0 \\ 0 \\ 0 \\ 0 \end{bmatrix}^{j-1}_t \,. \tag{65}$$

The diagonal part containing 1 shows the continuity of displacements in Eq.(63). Coefficients from T_1 to T_{11} show the stress continuity of Eq.(64) by means of displacements and temperature (and their derivatives in z). Eq.(65) in compact form is:

$$\boldsymbol{U}_b^j = \boldsymbol{T}_U^{j-1,j} \boldsymbol{U}_t^{j-1} + \boldsymbol{T}_\Theta^{j-1,j} \boldsymbol{\Theta}_t^{j-1} \,. \tag{66}$$

Eq.(66) is used to link displacements and their derivatives in z calculated at the bottom of the j layer with displacements and temperature (and also their derivatives in z) defined at the top of the (j-1) layer.

All the shells here considered are simply supported. Therefore, this condition is automatically satisfied by the harmonic forms used for all the variables:

$$w = v = 0,\ \sigma_{\alpha\alpha} = 0 \quad \text{for} \quad \alpha = 0, a\,, \tag{67}$$

$$w = u = 0,\ \sigma_{\beta\beta} = 0 \quad \text{for} \quad \beta = 0, b\,. \tag{68}$$

In the proposed benchmarks, no mechanical loads are applied at the external top and bottom surfaces of the shell. Therefore, using information from [79]- [83], these conditions in displacement form are defined as:

$$\boldsymbol{B}_t^M \boldsymbol{U}_t^M = \boldsymbol{P}_t^M = \boldsymbol{0}\,, \tag{69}$$

$$\boldsymbol{B}_b^1 \boldsymbol{U}_b^1 = \boldsymbol{P}_b^1 = \boldsymbol{0}\,, \tag{70}$$

subscripts t and b mean top and bottom, respectively. Superscript M indicates the last mathematical layer and superscript 1 indicates the first layer at the bottom. Vector $\boldsymbol{P}$ incudes the mechanical loads in the three direction α, β and z. This vector is zero in the present pure thermal stress analysis. Matrices $\boldsymbol{B}$ are used for the imposition of mechanical loads at the external surfaces. The explicit forms of $\boldsymbol{P}$ and $\boldsymbol{B}$ were already proposed in [79]- [83]. Eqs.(69) and (70) can be included in an algebraic system by means of their matrix form.

$\boldsymbol{U}_t^M = \boldsymbol{U}^M(h^M)$ is given in terms of $\boldsymbol{U}_b^1 = \boldsymbol{U}^1(0)$ for the pure mechanical analysis (displacements and their derivatives in $\tilde{z}$ at the top of the last layer are linked with the displacements and their derivatives in $\tilde{z}$ at the bottom of the first layer). For the thermo-mechanical analysis, further terms are included with respect to [79]- [83]. This aim is obtained by recursively introducing Eq.(66) into Eq.(62):

$$\begin{aligned}
\boldsymbol{U}_t^M = & \left(\boldsymbol{A}^{**M} \boldsymbol{T}_U^{M-1,M} \boldsymbol{A}^{**M-1} \boldsymbol{T}_U^{M-2,M-1} ..... \boldsymbol{A}^{**2} \boldsymbol{T}_U^{1,2} \boldsymbol{A}^{**1} \right) \boldsymbol{U}_b^1 + \\
& \Bigg(\boldsymbol{A}^{**M} \boldsymbol{T}_U^{M-1,M} \boldsymbol{A}^{**M-1} ..... \boldsymbol{A}^{**2} \boldsymbol{T}_U^{1,2} \boldsymbol{J}^{**1} + \\
& \boldsymbol{A}^{**M} \boldsymbol{T}_U^{M-1,M} \boldsymbol{A}^{**M-1} ..... \boldsymbol{A}^{**3} \boldsymbol{T}_U^{2,3} \boldsymbol{J}^{**2} + \\
& \vdots \\
& \boldsymbol{A}^{**M} \boldsymbol{T}_U^{M-1,M} \boldsymbol{J}^{**M-1} + \\
& \boldsymbol{J}^{**M} + \\
& \boldsymbol{A}^{**M} \boldsymbol{T}_U^{M-1,M} \boldsymbol{A}^{**M} ..... \boldsymbol{A}^{**2} \boldsymbol{T}_\Theta^{1,2} \boldsymbol{\Theta}_t^1 + \\
& \boldsymbol{A}^{**M} \boldsymbol{T}_U^{M-1,M} \boldsymbol{A}^{**M} ..... \boldsymbol{A}^{**3} \boldsymbol{T}_\Theta^{2,3} \boldsymbol{\Theta}_t^2 + \\
& \vdots \\
& \boldsymbol{A}^{**M} \boldsymbol{T}_U^{M-1,M} \boldsymbol{A}^{**M-1} \boldsymbol{T}_\Theta^{M-2,M-1} \boldsymbol{\Theta}_t^{M-2} + \\
& \boldsymbol{A}^{**M} \boldsymbol{T}_\Theta^{M-1,M} \boldsymbol{\Theta}_t^{M-1} \Bigg)\,.
\end{aligned} \tag{71}$$

The first block in parentheses in Eq.(71) indicates the 6×6 matrix $\boldsymbol{H}_m$ for multilayered structures already developed in [79]- [83] in the case of a pure mechanical analysis. M terms including $\boldsymbol{J}^{**j}$ (they

include the thermal profile within each j mathematical layer) and $M-1$ terms including $\boldsymbol{\Theta}_t^j$ (they include the temperature at each interface) are added. The summation of all these thermal quantities is included in the second block in brackets in Eq.(71). This block defines the vector $\boldsymbol{H}_\Theta$ of dimension 6×1. Therefore, the compact form of Eq.(71) is:

$$\boldsymbol{U}_t^M = \boldsymbol{H}_m \boldsymbol{U}_b^1 + \boldsymbol{H}_\Theta \,. \tag{72}$$

$\boldsymbol{H}_\Theta$ is the additional term with respect to the pure mechanical problem (see [79]- [83]).
Eq.(69) with $\boldsymbol{P}_t^M = 0$ is rewritten in terms of $\boldsymbol{U}_b^1$ using Eq.(72):

$$\boldsymbol{B}_t^M \boldsymbol{H}_m \boldsymbol{U}_b^1 = -\boldsymbol{B}_t^M \boldsymbol{H}_\Theta \,. \tag{73}$$

Eqs.(73) and (70) with $\boldsymbol{P}_b^1 = 0$ are given in compact form as:

$$\boldsymbol{E}\boldsymbol{U}_b^1 = \boldsymbol{P}_\Theta \,, \tag{74}$$

where

$$\boldsymbol{E} = \begin{bmatrix} \boldsymbol{B}_t^M \boldsymbol{H}_m \\ \boldsymbol{B}_b^1 \end{bmatrix} \tag{75}$$

and

$$\boldsymbol{P}_\Theta = \begin{bmatrix} -\boldsymbol{B}_t^M \boldsymbol{H}_\Theta \\ \boldsymbol{0} \end{bmatrix} . \tag{76}$$

Matrix $\boldsymbol{E}$ has always 6×6 dimension for each possible number M of mathematical layers and even if the method is based on a layer wise approach. This matrix is the same already seen for the pure mechanical analysis in [79]- [83]. A further development, to reduce the computational costs, could be the use of the Gaussian quadrature-type method for the numerical integration through the thickness of the shell without the use of the mathematical layers M. This powerful method was extensively applied and discussed in works [98]- [100]. A future numerical extension of the proposed model could be performed in accordance with the guidelines suggested in [98]- [100]. An alternative procedure could be also the use of the Generalized Differential Quadrature (GDQ) method in place of the exponential matrix method in order to solve the system of partial differential equations in z without the use of the mathematical layers M. The GDQ method was already used in works [101] and [102] for the implementation of a 3D GDQ shell model for the elastic static analysis of structures and it will be also extended to the thermal stress analysis of composite and FGM plates and shells in the near future.

The difference, with respect to the pure elastic analysis, is the load vector $\boldsymbol{P}_\Theta$ which contains only equivalent thermal loads. The system in Eq.(74) is formally the same developed in [79]- [83] for the pure mechanical analysis: the thermal field has been modified in an equivalent thermal load $\boldsymbol{P}_\Theta$ with dimension 6×1.

After the calculation of bottom displacements by means of Eq.(74), Eqs.(66) and (62) are used to calculate the displacements (and their derivatives with respect to z) through the entire thickness of the multilayered FGM plates and shells.

4 Results

The present section is split in two subsections. The first one is devoted to the validation of the present 3D exact model for plates and shells embedding FGM layers. The validation is conducted via the comparison with some past results found in the literature. This feature is useful to evaluate the appropriate number M of mathematical layers, to correctly consider both the curvature terms and the changing properties of the FGM layers, and the order of expansion N for the exponential matrix. After the validation of the model, new results will be presented in the second subsection. Using the

consolidated values of M and N, the present 3D solution is employed to see the effects of different calculated temperature profiles, thickness ratios, geometries, stacking sequences, possible inclusions of FGM layers. All the proposed assessments and benchmarks consider FGM layers with two constituent phases. The two considered phases are a metallic one (a Nickel-based Alloy known as Monel 70Ni-30Cu) and a ceramic one (Zirconia). The mechanical properties of each phase are given in terms of bulk modulus K and shear modulus G. The conductivity coefficient κ and the thermal expansion coefficient μ are also variable with the thickness coordinate $\tilde{z}$. The properties of metallic and ceramic phases are:

$$K_m = 227.24\,GPa, \quad G_m = 65.55\,GPa, \quad \mu_m = 15 \times 10^{-6}\,\frac{1}{K}, \quad \kappa_m = 25\,\frac{W}{mK}, \tag{77}$$

$$K_c = 125.83\,GPa, \quad G_c = 58.077\,GPa, \quad \mu_c = 10 \times 10^{-6}\,\frac{1}{K}, \quad \kappa_c = 2.09\,\frac{W}{mK}, \tag{78}$$

subscripts m and c indicate the metal and the ceramic phase, respectively. The volume fraction of the ceramic phase is assumed to follow a power law of order p:

$$V_c = \left(\tilde{z}_{_{FG}}/h_{_{FG}}\right)^p, \tag{79}$$

$h_{_{FG}}$ is the thickness of the FGM layer and $\tilde{z}_{_{FG}}$ is the local thickness coordinate for the FGM layer (it varies from 0 at the bottom surface to $h_{_{FG}}$ at the top surface). The generic FGM layer is fully metallic at its bottom and fully ceramic at its top because $V_c = 0$ when $\tilde{z}_{_{FG}} = 0$ and $V_c = 1$ when $\tilde{z}_{_{FG}} = h_{_{FG}}$.

The bulk and shear moduli are functions of the volume fraction of the ceramic phase V_c and they are estimated using the Mori-Tanaka model:

$$\frac{K - K_m}{K_c - K_m} = \frac{V_c}{1 + (1 - V_c)\frac{K_c - K_m}{K_m + \frac{4}{3}G_m}}, \quad \frac{G - G_m}{G_c - G_m} = \frac{V_c}{1 + (1 - V_c)\frac{G_c - G_m}{G_m + f_m}}, \quad f_m = \frac{G_m(9K_m + 8G_m)}{6(K_m + 2G_m)}\,. \tag{80}$$

The heat conduction coefficient κ is a function of the volume fraction of the ceramic phase:

$$\frac{\kappa - \kappa_m}{\kappa_c - \kappa_m} = \frac{V_c}{1 + (1 - V_c)\frac{\kappa_c - \kappa_m}{3\kappa_m}}\,. \tag{81}$$

The following relation is used to determine the effective thermal expansion coefficient μ:

$$\frac{\mu - \mu_m}{\mu_c - \mu_m} = \frac{\frac{1}{K} - \frac{1}{K_m}}{\frac{1}{K_c} - \frac{1}{K_m}}\,. \tag{82}$$

These material data were proposed in Reddy and Cheng [65] where all the missed details were given.

4.1 Preliminary validation

The new proposed 3D exact solution for plates and shells embedding FGM layers is validated by means of two preliminary assessments. A square plate and a cylindrical shell panel are investigated for different thickness ratios. The results obtained by means of the present 3D model are compared with those presented in the literature in terms of displacements and stresses. A number $M = 300$ of mathematical layers coupled with a third order expansion for the exponential matrix ($N = 3$) always gives results which are in very good accordance with those available in the literature. The two assessments consider structures with a single FGM layer. The bottom of the layer is fully metallic and the top one is fully ceramic. The results for these preliminary assessments are proposed in Tables 1 and 2. The displacements and stresses are given in non-dimensional form as:

$$\bar{u}_i = \frac{u_i}{Pa}, \quad \bar{\sigma}_{ij} = \frac{\sigma_{ij}}{PK^*}\,, \tag{83}$$

where $P = 10^{-6}$, $K^* = 1GPa$ and a is the dimension of shell or plate in α direction. i and j are equal to 1, 2 or 3 and they mean components $u_1 = u$, $u_2 = v$ and $u_3 = w$ for displacements and components $\sigma_{\alpha\alpha}$, $\sigma_{\beta\beta}$, σ_{zz}, $\sigma_{\alpha\beta}$, $\sigma_{\alpha z}$ and $\sigma_{\beta z}$ for stresses.

The first assessment shows a simply-supported square plate (a=b). The thickness ratio a/h can be 4, 10 or 50. A sovra-temperature field is imposed at the top (t) and at the bottom (b) surfaces by means of an harmonic field with half-wave numbers $m = n = 1$. The amplitudes of the sovra-temperature field are equal to $\Theta_t = +1K$ at the top and to $\Theta_b = 0K$ at the bottom. The plate is made of a single FGM layer ($h_{FG} = h$), whose mechanical and thermal properties were previously described in Eqs.(77)-(82). The volume fraction of the ceramic phase V_c is a quadratic function of the thickness coordinate ($p = 2$ in Eq.(79)). The 3D asymptotic method proposed by Reddy and Cheng [65] is assumed as the reference 3D solution. The results of the present 3D exact model have been obtained using an order of expansion $N = 3$ for the exponential matrix and different numbers M of mathematical layers to consider the variable elastic and thermal coefficients for the FGM layers. Table 1 shows displacement results for the thickness ratio $a/h = 4$, transverse shear and transverse normal stress results for the thickness ratio $a/h = 10$, and in-plane stress results for the thickness ratio $a/h = 50$. The results obtained by means of the new 3D shell solution can use an assumed linear temperature profile 3D(θ_a), a calculated temperature profile by means of the 1D simplified version of the Fourier heat conduction equation 3D(θ_c,1D), and a calculated temperature profile via the 3D Fourier equation 3D(θ_c,3D). For each temperature profile used in the analysis, the results show a consistent convergence when the number of mathematical layers M (used to approximate the variable elastic and thermal coefficients in the thickness direction) increases. Both the displacements and stresses obtained with the 3D(θ_c,3D) model, based on $M = 300$ mathematical layers, are coincident with the reference 3D solution by Reddy and Cheng [65]. The reference 3D solution [65] was also based on a 3D calculated temperature profile through the thickness. The results obtained via the 3D(θ_c,1D) model are quite different because the thermal conduction is considered only in the thickness direction (κ_3). This feature gives 3D(θ_c,1D) results quite different from the reference solution. The 3D(θ_a) model discards both the 3D thermal nature of the problem and the evolution of the thermal properties through the thickness direction. Therefore, 3D(θ_a) model is always quite different from the other proposed models. 3D(θ_c,3D) model is always in accordance with the 3D solution by Reddy and Cheng [65] for each thickness ratio and for each investigated variable.

The second assessment considers a simply supported cylindrical shell. The reference solution is the quasi-3D model proposed in [73] based on a 3D calculated temperature profile. The radii of curvature are $R_\alpha = \infty$ and $R_\beta = 10m$, while the in-plane dimensions are $a = 1m$ and $b = \frac{\pi}{3}R_\beta$. The thickness ratio R_β/h is equal to 50 or 1000. The thermal load is imposed at the external surfaces by means of a bi-sinusoidal ($m = n = 1$) sovra-temperature field with amplitudes $\Theta_t = +1K$ and $\Theta_b = 0K$ at the top and bottom surfaces, respectively. The power law of the volume fraction V_c through the thickness is quadratic ($p = 2$ in Eq.(79)). FGM law follows the Eqs.(77)-(82). In this new assessment, the mathematical layers are necessary to consider both the local elastic and thermal properties of the FGM layer and the parametric coefficients due to the curvature of the shell. Table 2 shows that the same order of expansion for the exponential matrix ($N = 3$) and the same number of mathematical layers ($M = 300$) proposed in the previous plate assessment are sufficient. The dimensionless displacements $\bar{w}$, $\bar{u}$ and dimensionless stress $\bar{\sigma}_{\beta\beta}$ are proposed at three different thickness coordinates; the dimensionless stresses $\bar{\sigma}_{\alpha z}$ and $\bar{\sigma}_{zz}$ are given at $\tilde{z} = h$ and $\tilde{z} = h/2$, respectively. The results given in terms of displacements and stresses via the 3D(θ_c,3D) model are in good accordance with the reference displacements and stresses in [73]. Showed small differences are due to the fact that the reference solution [73] is not a 3D solution but it is a quasi-3D model. The displacement and stress results have a stable behavior because they converge monotonically when the number M of mathematical layers increases. As stated in previous assessment, the 3D(θ_c,1D) model evaluates the material effect but it discards the 3D thickness layer effect. The linear assumption made for the 3D(θ_a)

model shows its inadequacy in the evaluation of the temperature profile in structures embedding FGM layers. When the thickness ratio R_β/h is 1000, the 3D(θ_c,1D) model applied to shells embedding a FGM layer is close to the 3D(θ_c,3D) model, and results show negligible differences. The 3D(θ_a) model always remains distant from the correct results.

4.2 Benchmarks

This subsection proposes four new benchmarks. Four geometries are investigated: plates, cylinders, cylindrical panels and spherical panels (see Figure 2 for further details). Different lamination schemes are presented where at least one FGM layer is embedded. Different FGM laws are considered in the four cases by changing the parameter p in Eqs.(77)-(82). Each benchmark is subjected to different sovra-temperature amplitudes and half-wave numbers. The results are presented for a wide range of thickness ratios (a/h for plates or R_α/h for shells) from 2 to 100. For each benchmark, the thermal stress analysis is achieved with three different temperature profile types. The 3D Fourier heat conduction equation is solved in order to determine the calculated temperature profile (θ_c,3D); the simplified 1D version of the previous heat conduction equation is used to define the calculated temperature profile (θ_c,1D); an assumed linear temperature profile (θ_a) is also used. As assessed in the previous subsection, the order of expansion for the exponential matrix is set equal to $N = 3$, and $M = 300$ mathematical layer are used. A detailed thermal stress analysis is proposed: it can be used as reference benchmarks for new 3D and 2D numerical and analytical models for plates and shells embedding FGM layers which will be developed in the future by other scientists.

The first benchmark investigates a simply-supported sandwich square plate with a FGM core. The in-plane dimensions are $a = b = 10m$; several thickness ratios are considered. The thickness of the top and bottom skins is the same ($h_1 = h_3 = 0.2h$); the FGM core is embedded in the remaining thickness portion ($h_2 = h_{FG} = 0.6h$). A bi-sinusoidal temperature ($m = n = 1$) is applied at the top and bottom surfaces with amplitudes $\Theta_t = +1.0K$ and $\Theta_b = -1.0K$. A quadratic evolution law ($p = 2$) is followed by the material volume fraction of the ceramic phase V_c inside the core (see properties in Eqs.(77)-(82)). Both the skins show constant elastic and thermal properties through the thickness; the top skin is fully ceramic and the bottom one is fully metallic. Figure 3 shows the volume fraction of the ceramic phase V_c and the bulk modulus K with respect to the non-dimensional thickness coordinate $\tilde{z}/h$. The typical sandwich configuration embedding a FGM core is clearly shown. The temperature profiles for the thicker and the thinner plate are presented in Figure 4. The (θ_c,3D) profile is the only able to consider both the thickness layer and the material layer effects. This feature is evident from the fact that it differs from the (θ_c,1D) profile in the case of thicker structure. The (θ_c,1D) profile is the same even if the thickness ratio changes; this feature is due to the fact that the 3D nature of the problem is discarded in the (θ_c,1D) profile, even if the local heat conduction coefficient κ_3 is considered. The (θ_a) profile assumes a priori linear temperature evaluation through the entire thickness. The three displacements and the six stress components are presented in Table 3 in particular thickness positions. Different thickness ratios are considered. As the thickness ratio a/h increases, the results given by the the 3D(θ_c,1D) model converge towards those given by the 3D(θ_c,3D) model. This feature is due to the fact that, as the thickness decreases, the 3D effect is smaller and the (θ_c,1D) temperature profile becomes a good approximation of the (θ_c,3D) one. The results obtained via the 3D(θ_a) model are always inadequate. Two displacements and four stresses are shown in Figure 5 for a thick ($a/h = 10$) plate. The typical 3D evaluations of displacements and stresses in a sandwich plate embedding a FGM core are proposed by means of the 3D($\theta_c, 3D$) model which is able to include all the 3D, material and thickness layer effects. Stresses $\sigma_{\alpha\alpha}$ and $\sigma_{\alpha\beta}$ are continuous at the skin-core interfaces because of the use of a FGM core which has graded elastic and thermal properties from those of the metallic bottom skin to those of the ceramic top skin. Transverse displacement w is not linear because of the FGM law and the small investigated thickness ratio a/h. Transverse shear stress $\sigma_{\beta z}$ and transverse normal

stress σ_{zz} satisfy the zero mechanical load conditions at the external surfaces.

The second benchmark considers a simply-supported one-layered FGM cylinder. The radii of curvature of this closed-section shell are $R_\alpha = 10m$ and $R_\beta = \infty$; the dimensions at the reference surface are $a = 2\pi R_\alpha$ and $b = 30m$ in α and β directions, respectively. The volume fraction of the ceramic phase V_c is assumed to evolve linearly through the thickness ($p = 1$); the bottom surface is fully metallic and the top surface is fully ceramic (see material laws in Eqs.(77)-(82)). An harmonic temperature distribution ($m = 2$; $n = 1$) is applied at the top and at the bottom surfaces; the sovra-temperature amplitudes are $\Theta_t = +1.0K$ and $\Theta_b = 0K$. The volume fraction of the ceramic phase V_c and the heat conduction coefficient κ are shown in Figure 6 as a function of the non-dimensional thickness coordinate $\tilde{z}/h$. The κ coefficient is not linear through the thickness, even if $p = 1$ is assumed, because of the particular form of Eq.(81). Figure 7 presents the temperature profiles for the cylinders with thickness ratios equal to $R_\alpha/h = 2$ and $R_\alpha/h = 100$. Negligible differences are shown between the (θ_c,3D) and the (θ_c,1D) profiles because of the symmetry of this closed and circular geometry: the structure is almost unaffected by the 3D effect even when the cylinder is really thick. As for the previous benchmark, the (θ_a) profile is distant from the other two profiles because it is a priori imposed as linear for the entire thickness of the FGM structure. Figure 8 shows the typical 3D displacement and stress evaluations through the thickness direction of a thick ($a/h = 10$) cylinder using the best possible model which is the 3D(θ_c,3D) one. $\sigma_{\alpha z}$ and σ_{zz} stresses fulfill the mechanical load boundary conditions (P_α=P_β=P_z=0). $\sigma_{\beta\beta}$ is continuous because only one layer is embedded in the structure. Transverse displacement w is not linear because of the FGM layer and its high thickness value. Table 4 shows displacements and stresses for different thickness ratios R_α/h. 3D(θ_c,3D) model and 3D(θ_c,1D) model are quite similar for thin cylinders. However, small differences are shown in the case of thicker cylinders because of the previous given explanations. 3D(θ_a) model is always inadequate for this thermal stress analysis because the hypothesis of linear temperature profile is not correct for FGM layers and for the proposed thickness ratios.

The third benchmark proposes a simply-supported sandwich cylindrical shell panel with FGM ($p = 0.5$) core. Material properties are proposed in Eqs.(77)-(82). As for the first benchmark, the FGM core has a thickness value $h_2 = h_{FG} = 0.6h$. The top skin is fully ceramic and the bottom one is fully metallic. The two skins have the same thickness $h_1 = h_3 = 0.2h$. The radii of curvature are the same used for the cylinder: $R_\alpha = 10m$ and $R_\beta = \infty$. The dimension in α direction is given in term of the radius of curvature and it is equal to $a = (\pi/3)R_\alpha$. The dimension in β direction is equal to $b = 30m$. The amplitudes of the external sovra-temperature are $\Theta_t = +1.0K$ and $\Theta_b = 0K$, the harmonic form of the temperature profile has half-wave numbers $m = 1$ and $n = 0$. The volume fraction of the ceramic phase V_c and the shear modulus G are given in Figure 9 where it is clearly shown the typical sandwich FGM configuration. Figure 10 shows the temperature profiles for a thick and a thin cylindrical panel. The correct temperature profile is always obtained by means of the 3D Fourier heat conduction equation even if the 1D version of the Fourier heat conduction equation is a good approximation (in particular for thin shells). The a priori linear assumed temperature profile is always inadequate. Figure 11 shows the typical 3D thermo-mechanical behavior, in terms of displacements and stresses, for a thick sandwich cylindrical shell embedding a FGM core. $\sigma_{\alpha z}$ and σ_{zz} are zero at the external surfaces because no mechanical P_α and P_z loads have been applied. $\sigma_{\alpha\alpha}$ and $\sigma_{\beta\beta}$ are continuous at the skin-core interfaces because of the use of the FGM central core. The evolutions of the investigated variables reproduce, as behavior, the employed FGM law. The 3D(θ_c,3D) model correctly works for all the investigated variables. Table 5 proposes displacements and stresses (in different positions through the thickness) for several thickness ratios. The 3D(θ_a) model is always inadequate because of the limitation given by the hypothesis of a priori assumed linear temperature profile. When the temperature profile is calculated (1D or 3D version), the results are very similar for thin cylindrical panels. For thicker shells, the use of 3D(θ_c,3D) model is mandatory. Displacement v and stresses $\sigma_{\alpha\beta}$ and $\sigma_{\beta z}$ are zero because half-wave number in β direction is zero ($n = 0$ has been imposed).

The fourth and last benchmark shows a simply-supported one-layered FGM ($p = 1$) spherical shell panel with material properties proposed in Eqs.(77)-(82). The radii of curvature are the same in α and β directions, and they are equal to $R_\alpha = R_\beta = 10m$. The dimensions are $a = (\pi/3)R_\alpha$ and $b = (\pi/3)R_\beta$. A wide range of thickness ratios is investigated: $R_\alpha/h = 2, 5, 10, 20, 50, 100$. The amplitudes of the external sovra-temperature field ($m = 2$, $n = 1$) are set as $\Theta_t = +0.5K$ and $\Theta_b = -0.5K$. Figure 12 allows to see how the volume fraction V_c of the ceramic phase and the thermal expansion coefficient μ evolve through the thickness direction. The thermal expansion coefficient μ is not linear in $\tilde{z}/h$, even if $p = 1$, because of the particular form used in Eq.(82). Figure 13 shows the temperature profiles for a thick and thin one-layered FGM spherical shell obtained via a linear assumption (θ_a), a 1D resolution of heat conduction problem (θ_c,1D) and a 3D resolution of heat conduction problem (θ_c,3D). The use of 3D Fourier heat conduction equation is mandatory for thick shells, while the 1D Fourier heat conduction problem is a good approximation for thinner shells. The linear assumed temperature profile is always inadequate for each thickness ratio. These considerations about the temperature profiles in Figure 13 have a confirmation in the displacement and stress results proposed in Table 6 for several thickness ratios: the 3D(θ_c,3D) model is always adequate, the 3D(θ_a) model is always inadequate, the 3D(θ_c,1D) model works properly only for thin and moderately thin spherical shells. Figure 14 shows the 3D evaluations for displacements and stresses in the case of thick one-layered FGM spherical shell. The graphics are obtained by means of the 3D(θ_c,3D) model which is the most suitable one to include the 3D, material and thickness layer effects. Transverse stresses satisfy the mechanical load boundary conditions. Displacements have a complicated form because of the FGM layer, spherical shell geometry and high thickness value. In-plane stresses are continuous because the shell is one-layered.

5 Conclusions

The proposed 3D shell solution in closed-form allows the thermal stress analysis of single-layered and sandwich plates, cylinders, cylindrical panels and spherical shells embedding Functionally Graded Material (FGM) layers. The temperature amplitude is imposed at the external surfaces in steady-state conditions. Then, the temperature profile through the thickness is defined by solving the 3D Fourier heat conduction equation (the relative thermo-mechanical model is called as 3D(θ_c,3D)), by solving the 1D Fourier heat conduction equation (the relative thermo-mechanical model is called as 3D(θ_c,1D)) or by assuming a priori the temperature profile as linear through the entire thickness of the structures (the relative thermo-mechanical model is called as 3D(θ_a)). The exponential matrix method was employed to solve the system of non-homogeneous second order differential equations in z which is given in closed form because of simply-supported boundary conditions and harmonic forms for displacements and temperature. The curvature of shells and the variable elastic and thermal coefficients of FGM layers give differential equations with non-constant coefficients. Constant coefficients for differential equations are obtained using mathematical layers and a layer wise approach. The 3D calculated temperature profile allows to consider both thickness layer and material layer effects, the 1D calculated temperature profile allows to consider only the material layer effect, the assumed linear temperature profile discards both these effects. The conducted analyses, in terms of displacements, stresses and temperature profiles, show that the use of a 3D calculated temperature profile is always necessary to perform a correct thermal stress investigation of plates and shells embedding FGM layers with different thickness ratios. A correct thermo-mechanical response is possible only if both the elastic part of the 3D shell model and the equivalent thermal load are correctly defined.

References

[1] K. Swaminathan and D.M. Sangeetha, Thermal analysis of FGM plates A critical review of various modeling techniques and solution methods, *Composite Structures*, 160, 43-60, 2017.

[2] K. Jayakrishna, V.R. Kar, M.T.H. Sultan and M. Rajesh, Materials selection for aerospace components, *Sustainable Composites for Aerospace Applications. Woodhead Publishing Series in Composites Science and Engineering*, 1, 1-18, 2018.

[3] L. Librescu and P. Marzocca, Thermal stresses '03, vol. 1, Blacksburg (VA, USA): Virginia Polytechnic Institute and State University, 2003.

[4] L. Librescu and P. Marzocca, Thermal stresses '03, vol. 2, Blacksburg (VA, USA): Virginia Polytechnic Institute and State University, 2003.

[5] A.K. Noor and W.S. Burton, Computational models for high-temperature multilayered composite plates and shells, *Applied Mechanics Reviews*, 45, 419-446, 1992.

[6] J.L. Nowinski, Theory of Thermoelasticity with Applications, The Netherlands: Sijthoff & Noordhoff, 1978.

[7] G.A. Altay and M.C. Dökmeci, Fundamental variational equations of discontinuous thermopiezoelectric fields, *International Journal of Engineering Science*, 34, 769-782, 1996.

[8] G.A. Altay and M.C. Dökmeci, Some variational principles for linear coupled thermoelasticity, *International Journal of Solids and Structures*, 33, 3937-3948, 1996.

[9] G.A. Altay and M.C. Dökmeci, Coupled thermoelastic shell equations with second sound for high-frequency vibrations of temperature-dependent materials, *International Journal of Solids and Structures*, 38, 2737-2768, 2001.

[10] A.A. Cannarozzi and F. Ubertini, A mixed variational method for linear coupled thermoelastic analysis, *International Journal of Solids and Structures*, 38, 717-739, 2001.

[11] N.C. Das, S.N. Das and B. Das, Eigenvalue approach to thermoelasticity, *Journal of Thermal Stresses*, 6, 35-43, 1983.

[12] W. Kosnski and K. Frischmuth, Thermomechanical coupled waves in a nonlinear medium, *Wave Motion*, 34, 131-141, 2001.

[13] J. Wauer, Free and forced magneto-thermo-elastic vibrations in a conducting plate layer, *Journal of Thermal Stresses*, 19, 671-691, 1996.

[14] S. Brischetto and R. Torre, Thermo-elastic analysis of multilayered plates and shells based on 1D and 3D heat conduction problems, *submitted*.

[15] K. Bhaskar, T.K. Varadan and J.S.M. Ali, Thermoelastic solution for orthotropic and anisotropic composite laminates, *Composites. Part B: Engineering*, 27, 415-420, 1996.

[16] N.J. Pagano, Exact solutions for composite laminates in cylindrical bending, *Journal of Composite Materials*, 3, 398-411, 1969.

[17] N.J. Pagano, Exact solutions for rectangular bidirectional composites and sandwich plates, *Journal of Composite Materials*, 4, 20-34, 1970.

[18] N.J. Pagano and A.S.D. Wang, Further study of composite laminates under cylindrical bending, *Journal of Composite Materials*, 5, 521-528, 1971.

[19] V.B. Tungikar and K.M. Rao, Three dimensional exact solution of thermal stresses in rectangular composite laminate, *Composite Structures*, 27, 419-430, 1994.

[20] M. Savoia and J.N. Reddy, Three-dimensional thermal analysis of laminated composite plates, *International Journal of Solids and Structures*, 32, 593-608, 1995.

[21] G.M. Kulikov and S.V. Plotnikova, Three-dimensional thermal stress analysis of laminated composite plates with general layups by a sampling surfaces method, *European Journal of Mechanics A/Solids*, 49, 214-226, 2015.

[22] S. Kapuria, S. Sengupta and P. C. Dumir, Three-dimensional solution for a hybrid cylindrical shell under axisymmetric thermoelectric load, *Archive of Applied Mechanics*, 67, 320-330, 1997.

[23] S. Kapuria, S. Sengupta and P.C. Dumir, Three-dimensional piezothermoelastic solution for shape control of cylindrical panel, *Journal of Thermal Stresses*, 20, 67-85, 1997.

[24] K. Xu and A.K. Noor, Three-dimensional analytical solutions for coupled thermoelectroelastic response of multi-layered cylindrical shells, *AIAA Journal*, 34, 802-812, 1996.

[25] W. Qu, Y. Zhang, Y. Gu and F. Wang, Three-dimensional thermal stress analysis using the indirect BEM in conjunction with the radial integration method, *Advances in Engineering Software*, 112, 147-153, 2017.

[26] Y. Ochiai, V. Sladek and J. Sladek, Three-dimensional unsteady thermal stress analysis by triple-reciprocity boundary element method, *Engineering Analysis with Boundary Elements*, 37, 116-127, 2013.

[27] R. Rolfes, J. Noack and M. Taeschner, High performance 3D-analysis of thermo-mechanically loaded composite structures, *Composite Structures*, 46, 367-379, 1999.

[28] J. Padovan, Thermoelasticity of cylindrically anisotropic generally laminated cylinders, *Journal of Applied Mechanics*, 43, 124-130, 1976.

[29] M. Tanaka, T. Matsumoto and M. Moradi, Application of boundary element method to 3-D problems of coupled thermoelasticity, *Engineering Analysis with Boundary Elements*, 16, 297-303, 1995.

[30] D. Trajkovski and R. Cukic, A coupled problem of thermoelastic vibrations of a circular plate with exact boundary conditions, *Mechanics Research Communications*, 26, 217-224, 1999.

[31] Y.-L. Yeh, The effect of thermo-mechanical coupling for a simply supported orthotropic rectangular plate on non-linear dynamics, *Thin-Walled Structures*, 43, 1277-1295, 2005.

[32] R.R. Das, A. Singla and S. Srivastava, Thermo-mechanical interlaminar stress and dynamic stability analysis of composite spherical shells, *Procedia Engineering*, 144, 1060-1066, 2016.

[33] A. Kalogeropoulos, G.A. Drosopoulos and G.E. Stavroulakis, Thermal-stress analysis of a three-dimensional end-plate steel joint, *Construction and Building Materials*, 29, 619-626, 2012.

[34] M. Bîrsan, Thermal stresses in cylindrical Cosserat elastic shells, *European Journal of Mechanics A/Solids*, 28, 94-101, 2009.

[35] R.K. Khare, T. Kant and A.K. Garg, Closed-form thermo-mechanical solutions of higher-order theories of cross-ply laminated shallow shells, *Composite Structures*, 59, 313-340, 2003.

[36] J.S.M. Ali, K. Bhaskar and T.K. Varadan, A new theory for accurate thermal/mechanical flexural analysis of symmetric laminated plates, *Composite Structures*, 45, 227-232, 1999.

[37] K.D. Jonnalagadda, T.R. Tauchert and G.E. Blandford, High-order thermoleastic composite plate theories: an analytic comparison, *Journal of Thermal Stresses*, 16, 265-285, 1993.

[38] A.A. Khdeir, Thermoelastic analysis of cross-ply laminated circular cylindrical shells, *International Journal of Solids and Structures*, 33, 4007-4016, 1996.

[39] A.A. Khdeir, M.D. Rajab and J.N. Reddy, Thermal effects on the response of cross-ply laminated shallow shells, *International Journal of Solids and Structures*, 29, 653-667, 1992.

[40] H. Murakami, Assessment of plate theories for treating the thermomechanical response of layered plates, *Composites Engineering*, 3, 137-149, 1993.

[41] W. Zhen and C. Wanji, A global-local higher order theory for multilayered shells and the analysis of laminated cylindrical shell panels, *Composite Structures*, 84, 350-361, 2008.

[42] S. Kapuria, P.C. Dumir and A. Ahmed, An efficient higher order zigzag theory for composite and sandwich beams subjected to thermal loading, *International Journal of Solids and Structures*, 40, 6613-6631, 2003.

[43] S. Brischetto, Effect of the through-the-thickness temperature distribution on the response of layered and composite shells, *International Journal of Applied Mechanics*, 1, 581-605, 2009.

[44] S. Brischetto and E. Carrera, Heat conduction and thermal analysis in multilayered plates and shells, *Mechanics Research Communications*, 38, 449-455, 2011.

[45] S. Brischetto, Hygrothermal loading effects in bending analysis of multilayered composite plates, *CMES: Computer Modeling in Engineering & Sciences*, 88, 367-417, 2012.

[46] S. Brischetto, Hygrothermoelastic analysis of multilayered composite and sandwich shells, *Journal of Sandwich Structures and Materials*, 15, 168-202, 2013.

[47] S. Brischetto and E. Carrera, Coupled thermo-mechanical analysis of one-layered and multilayered isotropic and composite shells, *CMES: Computer Modeling in Engineering & Sciences*, 56, 249-301, 2010.

[48] S. Brischetto and E. Carrera, Coupled thermo-mechanical analysis of one-layered and multilayered plates, *Composite Structures*, 92, 1793-1812, 2010.

[49] S. Brischetto and E. Carrera, Coupled thermo-electro-mechanical analysis of smart plates embedding composite and piezoelectric layers, *Journal of Thermal Stresses*, 35, 766-804, 2012.

[50] M. Cho and J. Oh, Higher order zig-zag theory for fully coupled thermo-electric-mechanical smart composite plates, *International Journal of Solids and Structures*, 41, 1331-1356, 2004.

[51] A. Barut, E. Madenci and A. Tessler, Nonlinear thermoelastic analysis of composite panels under non-uniform temperature distribution, *International Journal of Solids and Structures*, 37, 3681-3713, 2000.

[52] K.N. Cho, A.G. Striz and C.W. Bert, Thermal stress analysis of laminate using higher-order theory in each layer, *Journal of Thermal Stresses*, 12, 321-332, 1989.

[53] J.N. Reddy and Y.S. Hsu, Effects of shear deformation and anisotropy on the thermal bending of layered composite plates, *Journal of Thermal Stresses*, 3, 475-493, 1980.

[54] M. Jafari, M.B. Nazari and A. Taherinasab, Thermal stress analysis in metallic plates with a non-circular hole subjected to uniform heat flux, *European Journal of Mechanics A/Solids*, 59, 356-363, 2016.

[55] L. Librescu and W. Lin, Non-linear response of laminated plates and shells to thermomechanical loading: implications of violation of interlaminar shear traction continuity requirement, *International Journal of Solids and Structures*, 36, 4111-4147, 1999.

[56] C.J. Miller, W.A. Millavec and T.P. Kicher, Thermal stress analysis of layered cylindrical shells, *AIAA Journal*, 19, 523-530, 1981.

[57] Z.-Q. Cheng and R.C. Batra , Thermal effects on laminated composite shells containing interfacial imperfections, *Composite Structures*, 52, 3-11, 2001.

[58] R. Rolfes and K. Rohwer, Integrated thermal and mechanical analysis of composite plates and shells, *Composites Science and Technology*, 60, 2097-2106, 2000.

[59] D. Holstein, P. Aswendt, R. Höfling, C.-D. Schmidt and W. Jüptner, Deformation analysis of thermally loaded composite tubes, *Composite Structures*, 40, 257-265, 1998.

[60] K. Daneshjoo and M. Ramezani, Coupled thermoelasticity in laminated composite plates based on Green-Lindsay model, *Composite Structures*, 55, 387-392, 2002.

[61] K. Daneshjoo and M. Ramezani, Classical coupled thermoelasticity in laminated composite plates based on third-order shear deformation theory, *Composite Structures*, 64, 369-375, 2004.

[62] A. Ibrahimbegovic, J.B. Colliat and L. Davenne, Thermomechanical coupling in folded plates and non-smooth shells, *Computer Methods in Applied Mechanics Engineering*, 194, 2686-2707, 2005.

[63] Z.-Y. Lee, Generalized coupled transient thermoelastic problem of multilayered hollow cylinder with hybrid boundary conditions, *International Communications in Heat and Mass Transfer*, 33, 518-528, 2006.

[64] J. Oh and M. Cho, A finite element based on cubic zig-zag plate theory for the prediction of thermo-electric-mechanical behaviors, *International Journal of Solids and Structures*, 41, 1357-1375, 2004.

[65] J.N. Reddy and Z.-Q. Cheng, Three-dimensional thermomechanical deformations of functionally graded rectangular plates, *European Journal of Mechanics - A/Solids*, 20, 841-855, 2001.

[66] A. Alibeigloo and A.A. Pasha Zanoosi, Thermo-electro-elasticity solution of functionally graded carbon nanotube reinforced composite cylindrical shell embedded in piezoelectric layers, *Composite Structures*, 173, 268-280, 2017.

[67] S.S. Vel and J.L. Pelletier, Multi-objective optimization of functionally graded thick shells for thermal loading, *Composite Structures*, 81, 386-400, 2007.

[68] M. Adineh and M. Kadkhodayan, Three-dimensional thermo-elastic analysis and dynamic response of a multi-directional functionally graded skew plate on elastic foundation, *Composites. Part B: Engineering*, 125, 227-240, 2017.

[69] M. Dehghan, M.Z. Nejad and A. Moosaie, Thermo-electro-elastic analysis of functionally graded piezoelectric shells of revolution: governing equations and solutions for some simple cases, *International Journal of Engineering Science*, 104, 34-61, 2016.

[70] L. Wu, Z. Jiang and J. Liu, Thermoelastic stability of functionally graded cylindrical shells, *Composite Structures*, 70, 60-68, 2005.

[71] J.L. Pelletier and S.S. Vel, An exact solution for the steady-state thermoelastic response of functionally graded orthotropic cylindrical shells, *International Journal of Solids and Structures*, 43, 1131-1158, 2006.

[72] S. Brischetto, R. Leetsch, E. Carrera, T. Wallmersperger and B. Kröplin, Thermo-mechanical bending of functionally graded plates, *Journal of Thermal Stresses,*, 31, 286-308, 2008.

[73] M. Cinefra, E. Carrera, S. Brischetto and S. Belouettar, Thermo-mechanical analysis of functionally graded shells, *Journal of Thermal Stresses,*, 33, 942-963, 2010.

[74] H.-S. Shen, Postbuckling of axially loaded FGM hybrid cylindrical shells in thermal environments, *Composites Science and Technology*, 65, 1675-1690, 2005.

[75] H.-S. Shen and N. Noda, Postbuckling of pressure-loaded FGM hybrid cylindrical shells in thermal environments, *Composite Structures*, 77, 546-560, 2007.

[76] H.-S. Shen and N. Noda, Postbuckling of FGM cylindrical shells under combined axial and radial mechanical loads in thermal environments, *International Journal of Solids and Structures*, 42, 4641-4662, 2005.

[77] M. Jabbari, M.Z. Nejad and M. Ghannad, Thermo-elastic analysis of axially functionally graded rotating thick truncated conical shells with varying thickness, *Composites. Part B: Engineering*, 96, 20-34, 2016.

[78] H. Santos, C.M. Mota Soares, C.A. Mota Soares and J.N. Reddy, A semi-analytical finite element model for the analysis of cylindrical shells made of functionally graded materials under thermal shock, *Composite Structures*, 86, 10-21, 2008.

[79] S. Brischetto, An exact 3D solution for free vibrations of multilayered cross-ply composite and sandwich plates and shells, *International Journal of Applied Mechanics*, 6, 1-42, 2014.

[80] S. Brischetto, Exact three-dimensional static analysis of single- and multi-layered plates and shells, *Composites. Part B: Engineering*, 119, 230-252, 2017.

[81] S. Brischetto, A closed-form 3D shell solution for multilayered structures subjected to different load combinations, *Aerospace Science and Technology*, 70, 29-46, 2017.

[82] S. Brischetto, Convergence analysis of the exponential matrix method for the solution of 3D equilibrium equations for free vibration analysis of plates and shells, *Composites. Part B: Engineering*, 98, 453-471, 2017.

[83] S. Brischetto and R. Torre, Convergence investigation for the exponential matrix and mathematical layers in the static analysis of multilayered composite structures, *Journal of Composites Science*, 1, 1-15, 2017.

[84] S. Brischetto and R. Torre, Effects of order of expansion for the exponential matrix and number of mathematical layers in the exact 3D static analysis of functionally graded plates and shells, *Applied Sciences*, 8, 1-17, 2018.

[85] S. Brischetto, A 3D layer-wise model for the correct imposition of transverse shear/normal load conditions in FGM shells, *International Journal of Mechanical Sciences*, 136, 50-66, 2018.

[86] S. Brischetto, A general exact elastic shell solution for bending analysis of functionally graded structures, *Composite Structures*, 175, 70-85, 2017.

[87] S. Brischetto, Curvature approximation effects in the free vibration analysis of functionally graded shells, *International Journal of Applied Mechanics*, 8, 1-33, 2016.

[88] S. Brischetto, Exact elasticity solution for natural frequencies of functionally graded simply-supported structures, *Computer Modeling in Engineering and Sciences*, 95, 391-430, 2013.

[89] G.B. Arfken and H.J. Weber, Mathematical Methods for Physicists, Sixth Edition, Elsevier Academic Press, San Diego, USA, 2005.

[90] P.M. Morse and H. Feshbach, Methods of Theoretical Physics, McGraw-Hill, USA, 1953.

[91] M.N. Özişik, Heat Conduction, John Wiley & Sons, Inc., New York, 1993.

[92] Y. Povstenko, Fractional Thermoelasticity, Springer International Publishing, Switzerland, 2015.

[93] P. Moon and D.E. Spencer, Field Theory Handbook. Including Coordinate Systems, Differential Equations and Their Solutions, Springer-Verlag, Berlin, 1988.

[94] M.D. Mikhailov and M.N. Özişik, Unified Analysis and Solutions of Heat and Mass Diffusion, Dover Publications Inc., New York, 1984.

[95] A.W. Leissa, Vibration of Shells, NASA SP-288, Washington D.C., USA, 1973.

[96] W.E. Boyce and R.C. DiPrima, Elementary Differential Equations and Boundary Value Problems, John Wiley & Sons, Ltd., New York, 2001.

[97] Open document, Systems of Differential Equations, free available on http://www.math.utah.edu/gustafso/, accessed on 30th May 2013.

[98] L.F. Qian and R.C. Batra, Transient thermoelastic deformations of a thick functionally graded plate, *Journal of Thermal Stresses*, 27, 705-740, 2004.

[99] L.F. Qian, R.C. Batra and L.M. Chen, Analysis of cylindrical bending thermoelastic deformations of functionally graded plates by a meshless local Petrov-Galerkin method, *Computational Mechanics*, 33, 263-273, 2004.

[100] L.F. Qian, R.C. Batra and L.M. Chen, Static and dynamic deformations of thick functionally graded elastic plates by using higher-order shear and normal deformable plate theory and meshless local Petrov-Galerkin method, *Composites. Part B: Engineering*, 35, 685-697, 2004.

[101] S. Brischetto and F. Tornabene, Advanced GDQ models and 3D stress recovery in multilayered plates, spherical and double-curved panels subjected to transverse shear loads, *Composites. Part B: Engineering*, 146, 244-269, 2018.

[102] F. Tornabene and S. Brischetto, 3D capability of refined GDQ models for the bending analysis of composite and sandwich plates, spherical and doubly-curved shells, *Thin-Walled Structures*, 129, 94-124, 2018.

	Ref. 3D [65]	M=100	M=200	M=300	
		$a/h = 4$			
$\bar{w}(a/2, b/2)$ at $\tilde{z} = h$		4.284	4.284	4.284	3D(θ_a)
		3.208	3.207	3.207	3D(θ_c,1D)
	3.043	3.043	3.042	3.042	3D(θ_c,3D)
$\bar{w}(a/2, b/2)$ at $\tilde{z} = h/2$		2.784	2.784	2.784	3D(θ_a)
		2.227	2.226	2.226	3D(θ_c,1D)
	2.143	2.144	2.143	2.142	3D(θ_c,3D)
$\bar{w}(a/2, b/2)$ at $\tilde{z} = 0$		2.179	2.178	2.178	3D(θ_a)
		1.934	1.933	1.933	3D(θ_c,1D)
	1.901	1.901	1.900	1.900	3D(θ_c,3D)
$\bar{u}(0, b/2)$ at $\tilde{z} = h$		-2.631	-2.631	-2.631	3D(θ_a)
		-1.810	-1.809	-1.809	3D(θ_c,1D)
	-1.681	-1.681	-1.681	-1.680	3D(θ_c,3D)
$\bar{u}(0, b/2)$ at $\tilde{z} = h/2$		-1.3011	-1.3011	-1.3011	3D(θ_a)
		-0.7674	-0.7672	-0.7671	3D(θ_c,1D)
	-0.6822	-0.6822	-0.6819	-0.6819	3D(θ_c,3D)
$\bar{u}(0, b/2)$ at $\tilde{z} = 0$		-0.32522	-0.32524	-0.32525	3D(θ_a)
		0.02457	0.02449	0.02448	3D(θ_c,1D)
	0.08240	0.08256	0.08246	0.08245	3D(θ_c,3D)
		$a/h = 10$			
$\bar{\sigma}_{\alpha z}(0, b/2)$ at $\tilde{z} = h$		-1.323	-1.326	-1.326	3D(θ_a)
		1.514	1.510	1.509	3D(θ_c,1D)
	1.583	1.589	1.585	1.584	3D(θ_c,3D)
$\bar{\sigma}_{zz}(a/2, b/2)$ at $\tilde{z} = h/2$		-2.392	-2.392	-2.393	3D(θ_a)
		0.9173	0.9161	0.9158	3D(θ_c,1D)
	1.015	1.017	1.016	1.015	3D(θ_c,3D)
		$a/h = 50$			
$\bar{\sigma}_{\alpha\alpha}(a/2, b/2)$ at $\tilde{z} = h$		-493.2	-486.0	-483.6	3D(θ_a)
		-1018	-1011	-1008	3D(θ_c,1D)
	-1003	-1019	-1011	-1009	3D(θ_c,3D)
$\bar{\sigma}_{\alpha\alpha}(a/2, b/2)$ at $\tilde{z} = h/2$		-726.9	-724.9	-724.3	3D(θ_a)
		-253.5	-252.6	-252.3	3D(θ_c,1D)
	-251.2	-252.9	-252.0	-251.7	3D(θ_c,3D)
$\bar{\sigma}_{\alpha\alpha}(a/2, b/2)$ at $\tilde{z} = 0$		201.8	201.8	201.8	3D(θ_a)
		-75.89	-75.81	-75.80	3D(θ_c,1D)
	-76.10	-76.25	-76.16	-76.15	3D(θ_c,3D)

Table 1: First assessment, one-layered FGM plate ($a/b = 1$; $a/h = 4, 10, 50$; $p = 2$) with external sovra-temperature amplitudes $\Theta_t = +1K$ and $\Theta_b = 0K$ ($m = n = 1$). Reference solution is the 3D thermo-elastic model by Reddy and Cheng [65] based on a calculated 3D temperature profile through the thickness. New proposed 3D thermo-elastic solutions use order $N = 3$ for the exponential matrix and different M mathematical layers.

	Ref. [73]	M=100	M=200	M=300	
		$R_\beta/h = 50$			
$\bar{w}(a/2, b/2)$ at $\tilde{z} = h$		9.7762	9.7759	9.7759	3D(θ_a)
		7.2703	7.2676	7.2671	3D(θ_c,1D)
	7.1337	7.1358	7.1330	7.1325	3D(θ_c,3D)
$\bar{w}(a/2, b/2)$ at $\tilde{z} = h/2$		8.6365	8.6362	8.6362	3D(θ_a)
		6.5274	6.5250	6.5245	3D(θ_c,1D)
	6.4131	6.4150	6.4125	6.4120	3D(θ_c,3D)
$\bar{w}(a/2, b/2)$ at $\tilde{z} = 0$		8.1391	8.1388	8.1388	3D(θ_a)
		6.2932	6.2908	6.2903	3D(θ_c,1D)
	6.1942	6.1960	6.1936	6.1931	3D(θ_c,3D)
$\bar{u}(0, b/2)$ at $\tilde{z} = h$		-5.3821	-5.3820	-5.3820	3D(θ_a)
		-3.6438	-3.6426	-3.6423	3D(θ_c,1D)
	-3.5466	-3.5476	-3.5463	-3.5461	3D(θ_c,3D)
$\bar{u}(0, b/2)$ at $\tilde{z} = h/2$		-2.5642	-2.5642	-2.5642	3D(θ_a)
		-1.5131	-1.5127	-1.5126	3D(θ_c,1D)
	-1.4532	-1.4536	-1.4531	-1.4530	3D(θ_c,3D)
$\bar{u}(0, b/2)$ at $\tilde{z} = 0$		0.02374	0.02368	0.02367	3D(θ_a)
		0.4567	0.4565	0.45642	3D(θ_c,1D)
	0.4833	0.4835	0.4832	0.4832	3D(θ_c,3D)
		$R_\beta/h = 1000$			
$\bar{\sigma}_{\beta\beta}(a/2, b/2)$ at $\tilde{z} = h$		-560.36	-553.1	-550.7	3D(θ_a)
		-1175.3	-1167.5	-1164.8	3D(θ_c,1D)
	-1170.2	-1175.4	-1167.6	-1164.9	3D(θ_c,3D)
$\bar{\sigma}_{\beta\beta}(a/2, b/2)$ at $\tilde{z} = h/2$		-92.330	-90.79	-90.28	3D(θ_a)
		158.29	158.81	159.01	3D(θ_c,1D)
	159.55	158.33	158.85	159.05	3D(θ_c,3D)
$\bar{\sigma}_{\beta\beta}(a/2, b/2)$ at $\tilde{z} = 0$		1613.1	1613.1	1613.1	3D(θ_a)
		991.36	991.04	990.98	3D(θ_c,1D)
	991.05	991.27	990.95	990.89	3D(θ_c,3D)
$\bar{\sigma}_{\alpha z}(0, b/2)$ at $\tilde{z} = h$		-5.8888	-5.8888	-5.8887	3D(θ_a)
		-5.2257	-5.2238	-5.2234	3D(θ_c,1D)
	-5.2242	-5.2256	-5.2237	-5.2234	3D(θ_c,3D)
$\bar{\sigma}_{zz}(a/2, b/2)$ at $\tilde{z} = h/2$		0.2839	0.2839	0.2839	3D(θ_a)
		0.2393	0.2392	0.2392	3D(θ_c,1D)
	0.2428	0.2393	0.2392	0.2392	3D(θ_c,3D)

Table 2: Second assessment, one-layered FGM cylindrical shell ($R_\beta/h = 50, 1000$; $p = 2$) with external sovra-temperature amplitudes $\Theta_t = +1K$ and $\Theta_b = 0K$ ($m = n = 1$). Reference solution is the quasi-3D model in [73] based on a calculated 3D temperature profile through the thickness. New proposed 3D thermo-elastic solutions use order $N = 3$ for the exponential matrix and different M mathematical layers.

a/h	2	5	10	20	50	100
$u[10^{-4}\text{m}]$ at ($\alpha=0$, $\beta=b/2$, $\tilde{z}=0$)						
3D(θ_a)	0.3311	0.3034	0.2992	0.2981	0.2978	0.2978
3D(θ_c,1D)	0.4632	0.4104	0.4013	0.3989	0.3983	0.3982
3D(θ_c,3D)	0.3714	0.3925	0.3967	0.3978	0.3981	0.3981
$v[10^{-4}\text{m}]$ at ($\alpha=a/2$, $\beta=0$, $\tilde{z}=h$)						
3D(θ_a)	-0.2527	-0.2474	-0.2466	-0.2464	-0.2464	-0.2464
3D(θ_c,1D)	-0.02952	-0.05337	-0.05822	-0.05949	-0.05985	-0.05990
3D(θ_c,3D)	-0.1045	-0.06921	-0.06236	-0.06054	-0.06002	-0.05995
$w[10^{-4}\text{m}]$ at ($\alpha=a/2$, $\beta=b/2$, $\tilde{z}=h/2$)						
3D(θ_a)	0.2973	0.8475	1.723	3.459	8.658	17.32
3D(θ_c,1D)	0.2564	0.7166	1.452	2.913	7.289	14.58
3D(θ_c,3D)	0.2541	0.7140	1.451	2.912	7.289	14.58
$\sigma_{\alpha\alpha}[10^3\text{Pa}]$ at ($\alpha=a/2$, $\beta=b/2$, $\tilde{z}=0$)						
3D(θ_a)	1306	1553	1591	1601	1603	1604
3D(θ_c,1D)	127.7	598.7	679.8	700.7	706.6	707.4
3D(θ_c,3D)	946.7	757.8	720.8	711.0	708.2	707.8
$\sigma_{\beta\beta}[10^3\text{Pa}]$ at ($\alpha=a/2$, $\beta=b/2$, $\tilde{z}=h$)						
3D(θ_a)	-444.4	-480.4	-485.7	-487.0	-487.4	-487.5
3D(θ_c,1D)	-1957	-1795	-1763	-1754	-1752	-1751
3D(θ_c,3D)	-1449	-1688	-1735	-1747	-1750	-1751
$\sigma_{\alpha\beta}[10^3\text{Pa}]$ at ($\alpha=0$, $\beta=0$, $\tilde{z}=h/4$)						
3D(θ_a)	622.2	657.3	663.4	665.0	665.4	665.5
3D(θ_c,1D)	1130	1159	1165	1167	1167	1167
3D(θ_c,3D)	830.3	1091	1147	1162	1166	1167
$\sigma_{\alpha z}[10^3\text{Pa}]$ at ($\alpha=0$, $\beta=b/2$, $\tilde{z}=h/4$)						
3D(θ_a)	-47.72	-29.05	-15.36	-7.784	-3.126	-1.564
3D(θ_c,1D)	252.9	78.04	36.65	18.02	7.171	3.583
3D(θ_c,3D)	106.3	65.40	35.00	17.81	7.157	3.581
$\sigma_{\beta z}[10^3\text{Pa}]$ at ($\alpha=a/2$, $\beta=0$, $\tilde{z}=3h/4$)						
3D(θ_a)	68.09	34.46	17.83	8.988	3.604	1.802
3D(θ_c,1D)	-259.4	-84.31	-40.11	-19.79	-7.883	-3.939
3D(θ_c,3D)	-117.4	-71.94	-38.49	-19.58	-7.870	-3.938
$\sigma_{zz}[10^3\text{Pa}]$ at ($\alpha=a/2$, $\beta=b/2$, $\tilde{z}=3h/4$)						
3D(θ_a)	-40.56	-7.168	-1.820	-0.4569	-0.07318	-0.01830
3D(θ_c,1D)	161.1	21.86	5.257	1.301	0.2075	0.05185
3D(θ_c,3D)	83.55	19.17	5.081	1.290	0.2072	0.05183

Table 3: First benchmark, simply-supported sandwich square plate with FGM ($p=2$) core. External sovra-temperature amplitudes $\Theta_t=+1.0K$ and $\Theta_b=-1.0K$ ($m=n=1$). Proposed 3D thermo-elastic solutions use order $N=3$ for the exponential matrix and $M=300$ mathematical layers.

R_α/h	2	5	10	20	50	100
$u[10^{-4}\text{m}]$ at ($\alpha = 0$, $\beta = b/2$, $\tilde{z} = 0$)						
3D(θ_a)	0.7546	0.6504	0.5895	0.5551	0.5334	0.5260
3D(θ_c,1D)	0.5108	0.4101	0.3605	0.3337	0.3171	0.3116
3D(θ_c,3D)	0.4962	0.4077	0.3600	0.3336	0.3171	0.3115
$v[10^{-4}\text{m}]$ at ($\alpha = a/2$, $\beta = 0$, $\tilde{z} = h$)						
3D(θ_a)	-0.9190	-0.6968	-0.6177	-0.5795	-0.5574	-0.5502
3D(θ_c,1D)	-0.5850	-0.4227	-0.3690	-0.3438	-0.3295	-0.3249
3D(θ_c,3D)	-0.5656	-0.4201	-0.3683	-0.3437	-0.3295	-0.3249
$w[10^{-4}\text{m}]$ at ($\alpha = a/2$, $\beta = b/2$, $\tilde{z} = h/2$)						
3D(θ_a)	1.175	1.166	1.134	1.112	1.098	1.093
3D(θ_c,1D)	0.7513	0.7154	0.6830	0.6632	0.6504	0.6460
3D(θ_c,3D)	0.7268	0.7110	0.6819	0.6630	0.6504	0.6460
$\sigma_{\alpha\alpha}[10^3\text{Pa}]$ at ($\alpha = a/2$, $\beta = b/2$, $\tilde{z} = 0$)						
3D(θ_a)	1223	1512	1575	1598	1609	1612
3D(θ_c,1D)	779.8	925.0	947.1	951.9	952.8	952.8
3D(θ_c,3D)	754.0	919.3	945.5	951.5	952.8	952.8
$\sigma_{\beta\beta}[10^3\text{Pa}]$ at ($\alpha = a/2$, $\beta = b/2$, $\tilde{z} = h$)						
3D(θ_a)	-166.8	-609.9	-773.7	-854.5	-901.9	-917.5
3D(θ_c,1D)	-887.9	-1216	-1330	-1384	-1416	-1426
3D(θ_c,3D)	-929.8	-1222	-1331	-1385	-1416	-1426
$\sigma_{\alpha\beta}[10^3\text{Pa}]$ at ($\alpha = 0$, $\beta = 0$, $\tilde{z} = h/4$)						
3D(θ_a)	153.3	77.86	40.40	20.39	8.178	4.090
3D(θ_c,1D)	131.2	60.56	30.57	15.22	6.058	3.022
3D(θ_c,3D)	129.5	60.36	30.54	15.22	6.058	3.022
$\sigma_{\alpha z}[10^3\text{Pa}]$ at ($\alpha = 0$, $\beta = b/2$, $\tilde{z} = h/4$)						
3D(θ_a)	-76.60	-46.07	-25.19	-13.06	-5.322	-2.676
3D(θ_c,1D)	-62.35	-33.72	-17.93	-9.170	-3.709	-1.860
3D(θ_c,3D)	-61.13	-33.57	-17.91	-9.167	-3.708	-1.860
$\sigma_{\beta z}[10^3\text{Pa}]$ at ($\alpha = a/2$, $\beta = 0$, $\tilde{z} = 3h/4$)						
3D(θ_a)	-16.01	-28.25	-17.96	-9.886	-4.162	-2.114
3D(θ_c,1D)	-53.80	-36.87	-20.89	-11.00	-4.523	-2.281
3D(θ_c,3D)	-55.68	-36.93	-20.90	-11.00	-4.523	-2.281
$\sigma_{zz}[10^3\text{Pa}]$ at ($\alpha = a/2$, $\beta = b/2$, $\tilde{z} = 3h/4$)						
3D(θ_a)	42.64	30.20	17.74	9.557	3.989	2.023
3D(θ_c,1D)	68.61	36.78	20.16	10.53	4.321	2.179
3D(θ_c,3D)	69.86	36.82	20.17	10.53	4.321	2.179

Table 4: Second benchmark, simply-supported one-layered FGM ($p = 1$) cylinder. External sovra-temperature amplitudes $\Theta_t = +1.0K$ and $\Theta_b = 0K$ ($m = 2$, $n = 1$). Proposed 3D thermo-elastic solutions use order $N = 3$ for the exponential matrix and $M = 300$ mathematical layers.

R_α/h	2	5	10	20	50	100
$u[10^{-4}\text{m}]$ at ($\alpha = 0$, $\beta = b/2$, $\tilde{z} = 0$)						
3D(θ_a)	-0.01519	0.1631	0.4185	0.9187	2.413	4.901
3D(θ_c,1D)	0.1130	0.2736	0.5134	0.9863	2.401	4.758
3D(θ_c,3D)	0.1194	0.2738	0.5131	0.9860	2.401	4.758
$v[10^{-4}\text{m}]$ at ($\alpha = a/2$, $\beta = 0$, $\tilde{z} = h$)						
3D(θ_a)	0.0000	0.0000	0.0000	0.0000	0.0000	0.0000
3D(θ_c,1D)	0.0000	0.0000	0.0000	0.0000	0.0000	0.0000
3D(θ_c,3D)	0.0000	0.0000	0.0000	0.0000	0.0000	0.0000
$w[10^{-4}\text{m}]$ at ($\alpha = a/2$, $\beta = b/2$, $\tilde{z} = h/2$)						
3D(θ_a)	0.2096	0.6493	1.396	2.890	7.370	14.83
3D(θ_c,1D)	0.2307	0.6588	1.368	2.784	7.026	14.10
3D(θ_c,3D)	0.2275	0.6558	1.366	2.783	7.026	14.10
$\sigma_{\alpha\alpha}[10^3\text{Pa}]$ at ($\alpha = a/2$, $\beta = b/2$, $\tilde{z} = 0$)						
3D(θ_a)	403.3	267.2	259.3	262.1	265.7	267.2
3D(θ_c,1D)	-378.5	-399.6	-388.2	-379.4	-373.1	-370.9
3D(θ_c,3D)	-424.6	-406.3	-389.9	-379.8	-373.2	-370.9
$\sigma_{\beta\beta}[10^3\text{Pa}]$ at ($\alpha = a/2$, $\beta = b/2$, $\tilde{z} = h$)						
3D(θ_a)	-1460	-1497	-1500	-1500	-1499	-1499
3D(θ_c,1D)	-1655	-1681	-1684	-1684	-1683	-1683
3D(θ_c,3D)	-1680	-1686	-1685	-1684	-1683	-1683
$\sigma_{\alpha\beta}[10^3\text{Pa}]$ at ($\alpha = 0$, $\beta = 0$, $\tilde{z} = h/4$)						
3D(θ_a)	0.0000	0.0000	0.0000	0.0000	0.0000	0.0000
3D(θ_c,1D)	0.0000	0.0000	0.0000	0.0000	0.0000	0.0000
3D(θ_c,3D)	0.0000	0.0000	0.0000	0.0000	0.0000	0.0000
$\sigma_{\alpha z}[10^3\text{Pa}]$ at ($\alpha = 0$, $\beta = b/2$, $\tilde{z} = h/4$)						
3D(θ_a)	-38.43	-8.765	-4.156	-2.117	-0.8687	-0.4390
3D(θ_c,1D)	60.02	27.61	13.70	6.758	2.672	1.330
3D(θ_c,3D)	67.48	28.11	13.77	6.765	2.672	1.330
$\sigma_{\beta z}[10^3\text{Pa}]$ at ($\alpha = a/2$, $\beta = 0$, $\tilde{z} = 3h/4$)						
3D(θ_a)	0.0000	0.0000	0.0000	0.0000	0.0000	0.0000
3D(θ_c,1D)	0.0000	0.0000	0.0000	0.0000	0.0000	0.0000
3D(θ_c,3D)	0.0000	0.0000	0.0000	0.0000	0.0000	0.0000
$\sigma_{zz}[10^3\text{Pa}]$ at ($\alpha = a/2$, $\beta = b/2$, $\tilde{z} = 3h/4$)						
3D(θ_a)	-17.98	-3.253	-1.431	-0.7036	-0.2825	-0.1417
3D(θ_c,1D)	33.76	12.50	5.614	2.608	0.9907	0.4862
3D(θ_c,3D)	38.27	12.74	5.641	2.611	0.9909	0.4863

Table 5: Third benchmark, simply-supported sandwich cylindrical shell panel with FGM ($p = 0.5$) core. External sovra-temperature amplitudes $\Theta_t = +1.0K$ and $\Theta_b = 0K$ ($m = 1$, $n = 0$). Proposed 3D thermo-elastic solutions use order $N = 3$ for the exponential matrix and $M = 300$ mathematical layers.

R_α/h	2	5	10	20	50	100
$u[10^{-4}\text{m}]$ at ($\alpha = 0$, $\beta = b/2$, $\tilde{z} = 0$)						
3D(θ_a)	0.1463	0.1361	0.1176	0.07489	0.02761	0.01223
3D(θ_c,1D)	0.1845	0.1482	0.1092	0.05599	0.01413	0.004601
3D(θ_c,3D)	0.1328	0.1412	0.1086	0.05608	0.01415	0.004604
$v[10^{-4}\text{m}]$ at ($\alpha = a/2$, $\beta = 0$, $\tilde{z} = h$)						
3D(θ_a)	-0.05093	-0.03120	-0.01019	0.007458	0.009691	0.006075
3D(θ_c,1D)	-0.01403	0.0008737	0.01793	0.02612	0.01696	0.009394
3D(θ_c,3D)	-0.02979	-0.004143	0.01656	0.02585	0.01694	0.009392
$w[10^{-4}\text{m}]$ at ($\alpha = a/2$, $\beta = b/2$, $\tilde{z} = h/2$)						
3D(θ_a)	0.04248	0.1429	0.2121	0.1867	0.06217	-0.002022
3D(θ_c,1D)	0.02303	0.09350	0.1006	-0.001929	-0.1711	-0.2395
3D(θ_c,3D)	0.03415	0.09846	0.1047	0.0002098	-0.1706	-0.2393
$\sigma_{\alpha\alpha}[10^3\text{Pa}]$ at ($\alpha = a/2$, $\beta = b/2$, $\tilde{z} = 0$)						
3D(θ_a)	77.92	699.0	1176	16.79	1948	1699
3D(θ_c,1D)	-477.5	447.2	1002	1410	1470	1395
3D(θ_c,3D)	260.7	544.6	1019	1415	1471	1395
$\sigma_{\beta\beta}[10^3\text{Pa}]$ at ($\alpha = a/2$, $\beta = b/2$, $\tilde{z} = h$)						
3D(θ_a)	-396.8	-418.6	-498.4	-742.6	-1041	-1145
3D(θ_c,1D)	-870.5	-894.8	-1050	-1354	-1624	-1694
3D(θ_c,3D)	-673.4	-827.2	-1026	-1346	-1623	-1694
$\sigma_{\alpha\beta}[10^3\text{Pa}]$ at ($\alpha = 0$, $\beta = 0$, $\tilde{z} = h/4$)						
3D(θ_a)	275.8	328.1	321.7	321.3	98.09	46.74
3D(θ_c,1D)	430.6	416.0	349.5	212.0	73.14	31.17
3D(θ_c,3D)	260.1	387.3	345.2	211.7	73.16	31.17
$\sigma_{\alpha z}[10^3\text{Pa}]$ at ($\alpha = 0$, $\beta = b/2$, $\tilde{z} = h/4$)						
3D(θ_a)	-49.42	-78.39	-89.82	-76.52	-38.51	-19.78
3D(θ_c,1D)	71.74	-70.19	-95.94	-75.30	-33.19	-15.99
3D(θ_c,3D)	-12.37	-71.98	-95.28	-75.21	-33.19	-15.99
$\sigma_{\beta z}[10^3\text{Pa}]$ at ($\alpha = a/2$, $\beta = 0$, $\tilde{z} = 3h/4$)						
3D(θ_a)	-0.03903	-14.50	-27.11	-27.80	-15.03	-7.836
3D(θ_c,1D)	-103.5	-65.39	-56.15	-40.64	-18.03	-8.818
3D(θ_c,3D)	-32.23	-54.35	-54.25	-40.39	-18.02	-8.816
$\sigma_{zz}[10^3\text{Pa}]$ at ($\alpha = a/2$, $\beta = b/2$, $\tilde{z} = 3h/4$)						
3D(θ_a)	43.86	28.63	23.58	18.72	9.697	5.106
3D(θ_c,1D)	186.8	65.12	39.91	25.62	11.39	5.687
3D(θ_c,3D)	90.90	56.74	38.75	25.48	11.38	5.686

Table 6: Fourth benchmark, simply-supported one-layered FGM ($p = 1$) spherical shell panel. External sovra-temperature amplitudes $\Theta_t = +0.5K$ and $\Theta_b = -0.5K$ ($m = 2$, $n = 1$). Proposed 3D thermo-elastic solutions use order $N = 3$ for the exponential matrix and $M = 300$ mathematical layers.

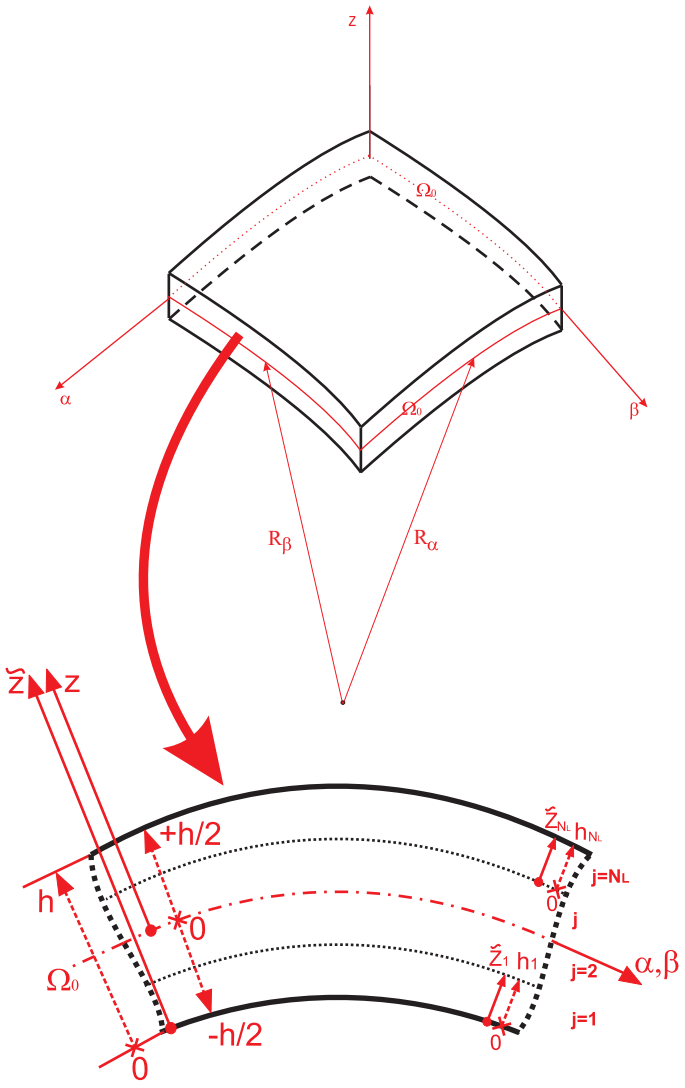

Figure 1: Geometrical elements and notations for a generic spherical shell.

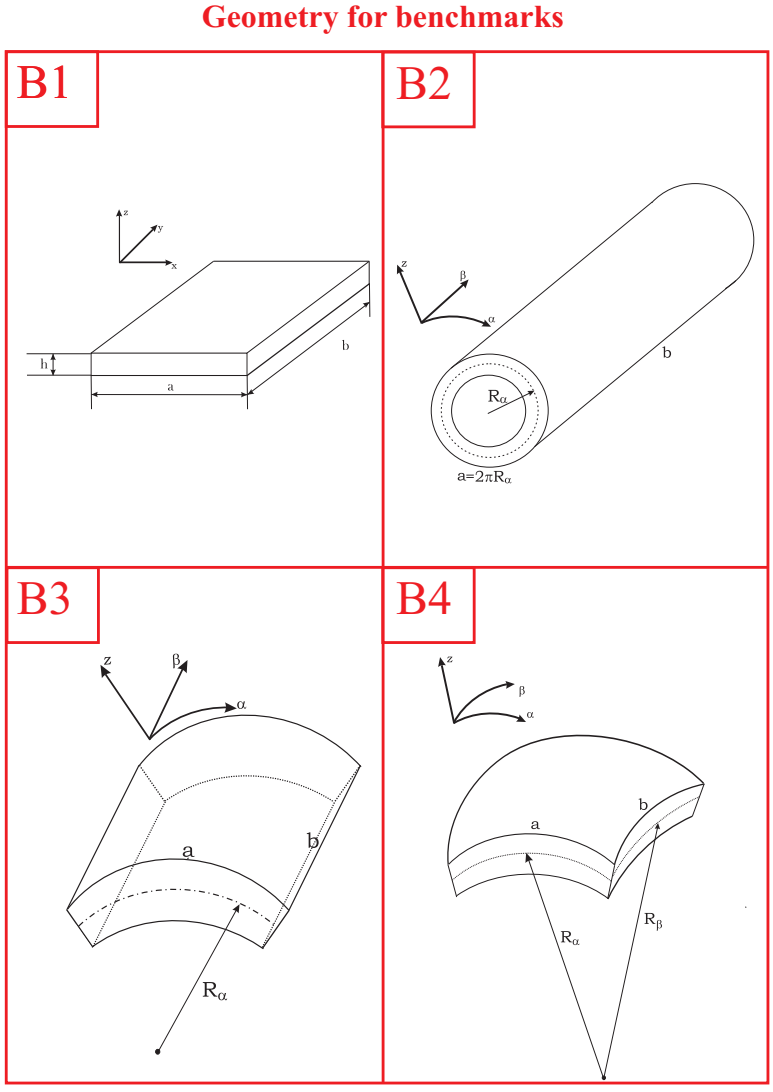

Figure 2: Geometry of the four investigated benchmarks: plate (B1), cylinder (B2), cylindrical shell (B3) and spherical shell (B4).

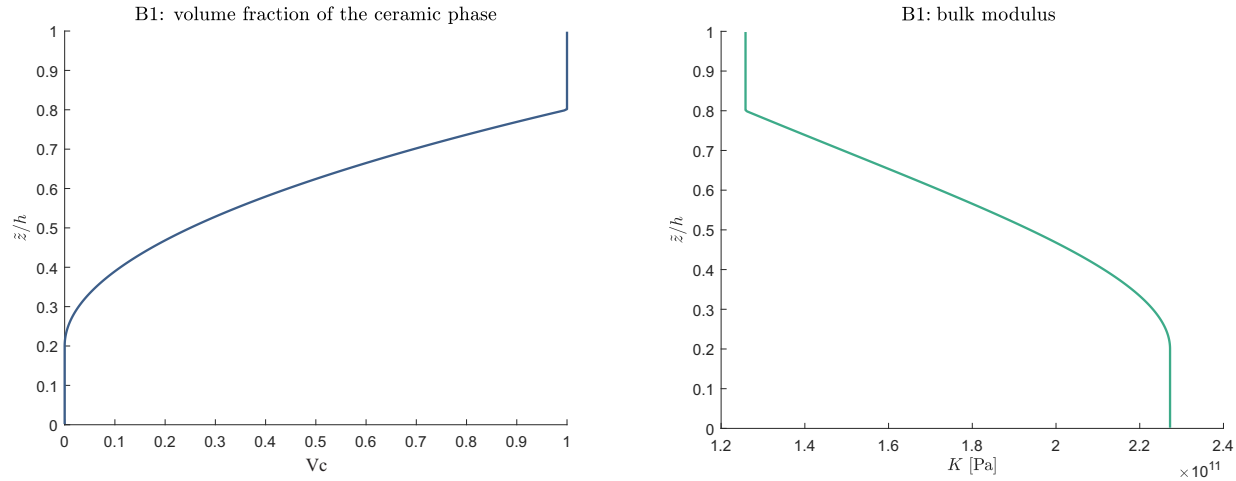

Figure 3: First benchmark, volume fraction of the ceramic phase V_c (on the left) and bulk modulus K (on the right) evaluated through the thickness of the sandwich square plate with FGM ($p = 2$) core.

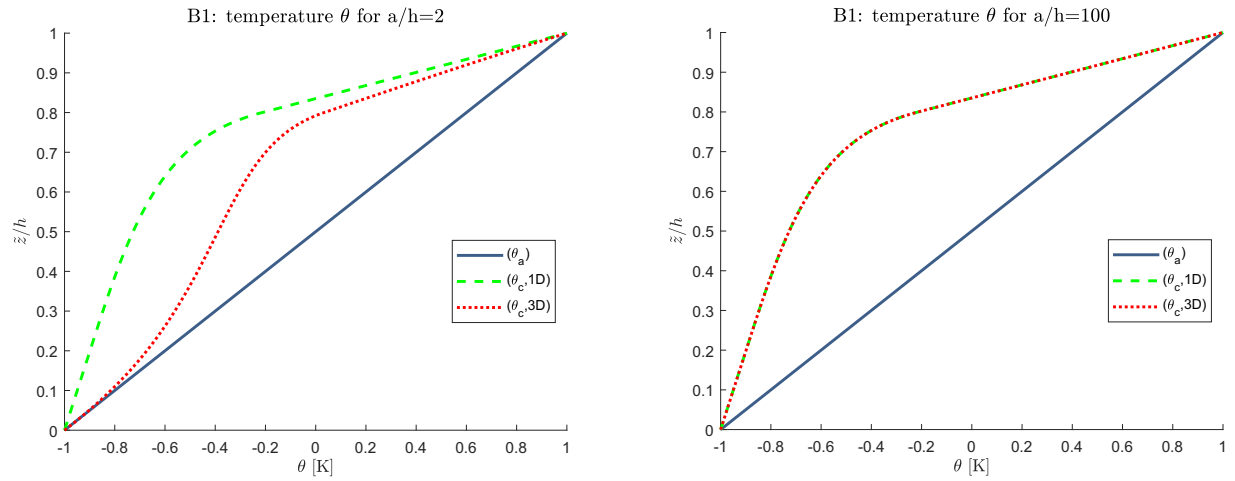

Figure 4: First benchmark, temperature profiles for thick (on the left) and thin (on the right) sandwich square plate with FGM ($p = 2$) core. The maximum amplitude of the temperature $\theta(\alpha, \beta, z)$ is evaluated at (a/2,b/2).

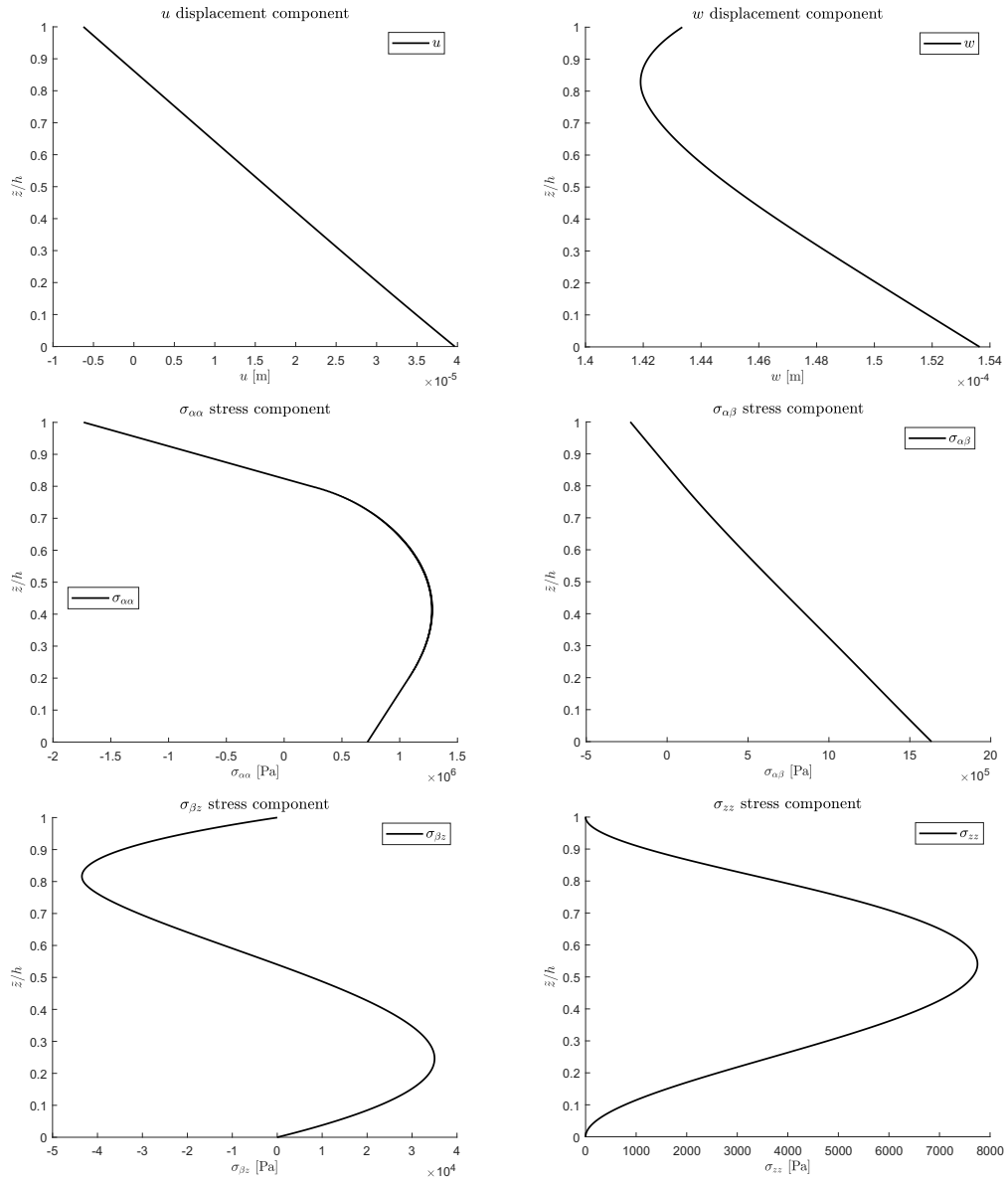

Figure 5: First benchmark, displacements and stresses for thick (a/h=10) sandwich square plate with FGM ($p = 2$) core obtained via a 3D exact model based on a 3D calculated temperature profile 3D(θ_c,3D). Maximum amplitudes: u at (0,b/2); w, $\sigma_{\alpha\alpha}$ and σ_{zz} at (a/2,b/2); $\sigma_{\alpha\beta}$ at (0,0); $\sigma_{\beta z}$ at (a/2,0).

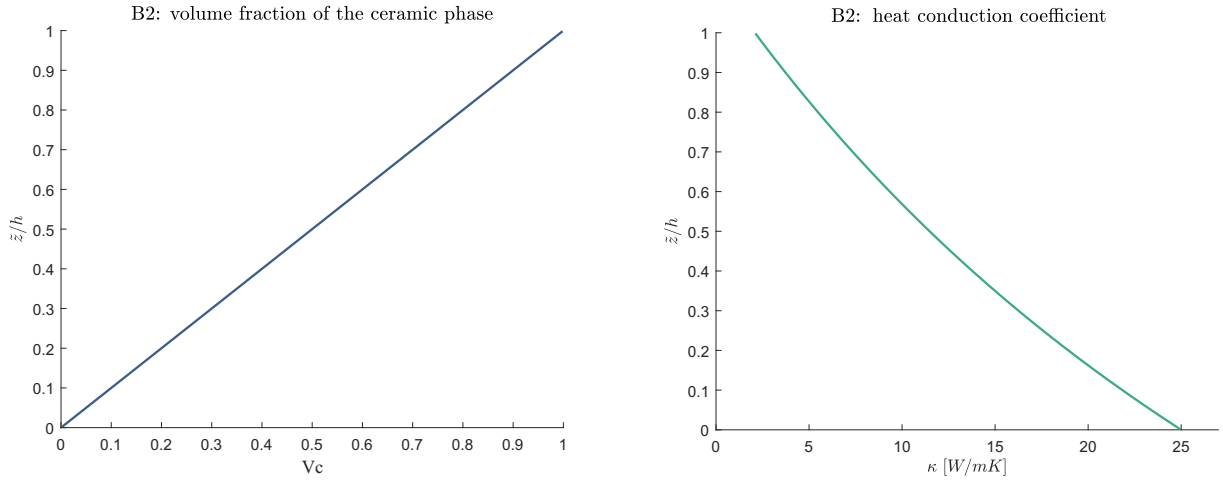

Figure 6: Second benchmark, volume fraction of the ceramic phase V_c (on the left) and heat conduction coefficient κ (on the right) evaluated through the thickness of the one-layered FGM ($p = 1$) cylinder.

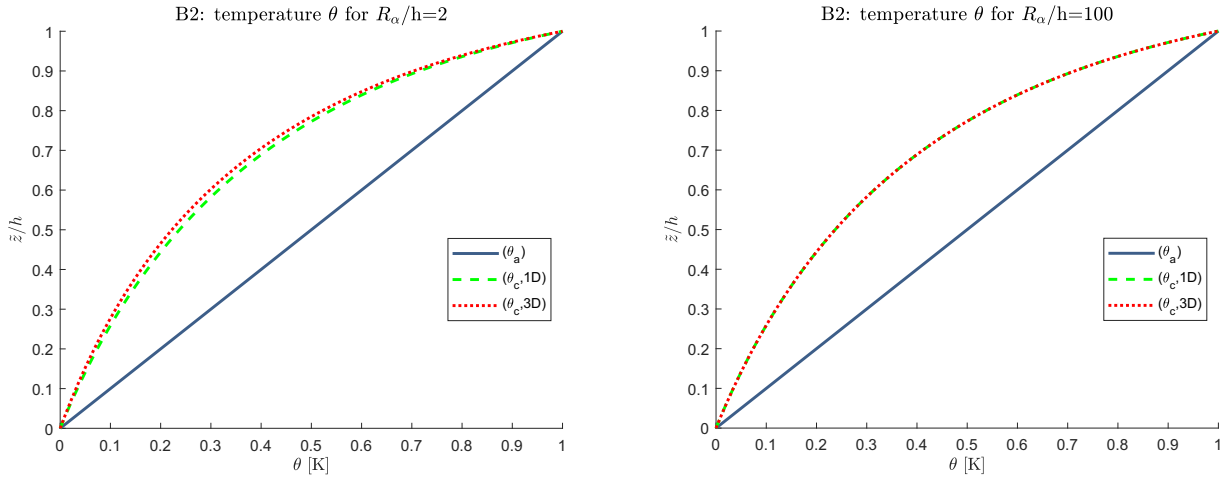

Figure 7: Second benchmark, temperature profiles for thick (on the left) and thin (on the right) one-layered FGM ($p = 1$) cylinder. The maximum amplitude of the temperature $\theta(\alpha, \beta, z)$ is evaluated at (a/2,b/2).

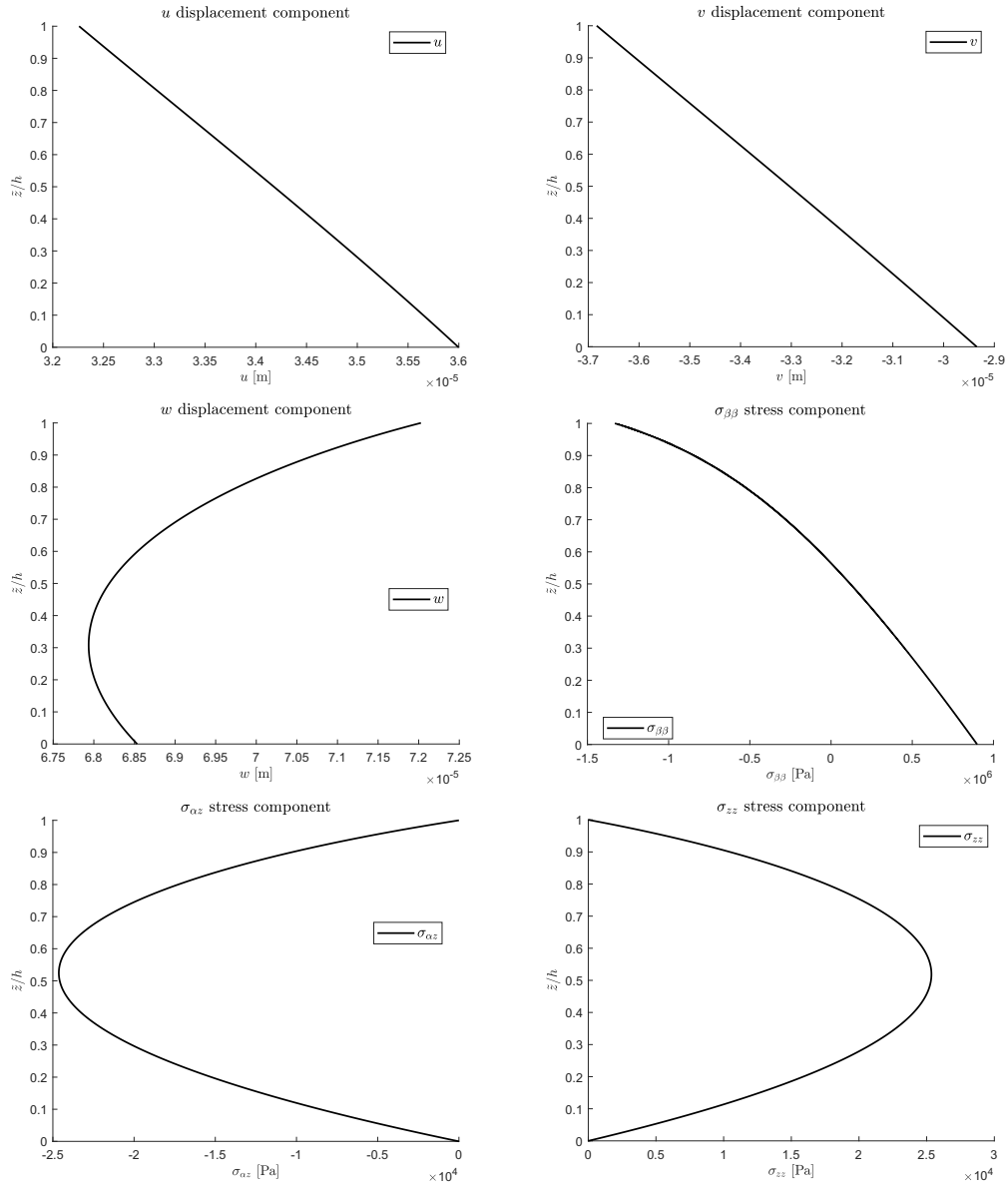

Figure 8: Second benchmark, displacements and stresses for thick (R_α/h=10) one-layered FGM ($p = 1$) cylinder obtained via a 3D exact model based on a 3D calculated temperature profile 3D(θ_c,3D). Maximum amplitudes: u and $\sigma_{\alpha z}$ at (0,$b/2$); v at ($a/2$,0); w, $\sigma_{\beta\beta}$ and σ_{zz} at ($a/2$,$b/2$).

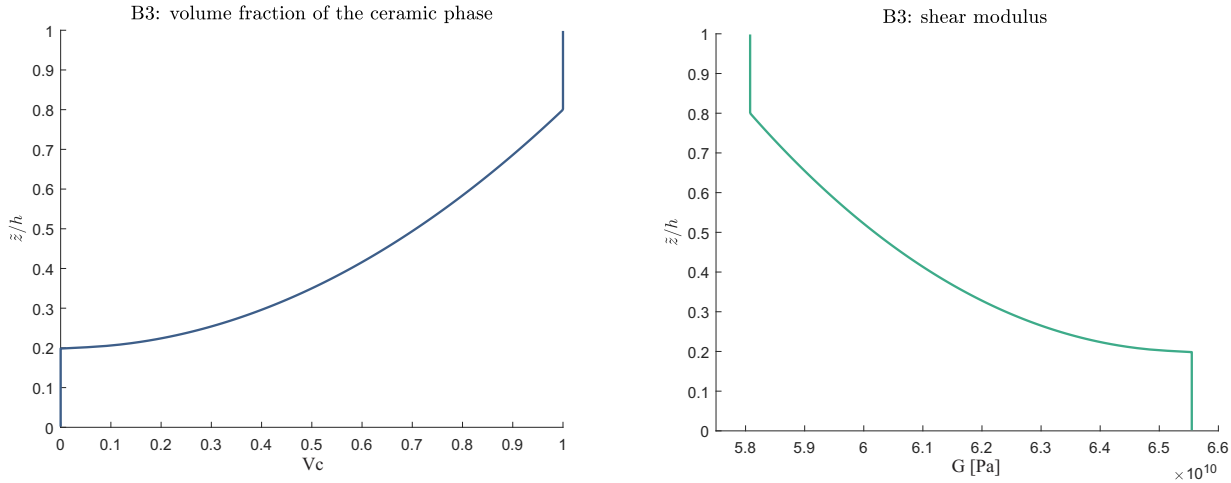

Figure 9: Third benchmark, volume fraction of the ceramic phase V_c (on the left) and shear modulus G (on the right) evaluated through the thickness of the sandwich cylindrical shell panel with FGM ($p = 0.5$) core.

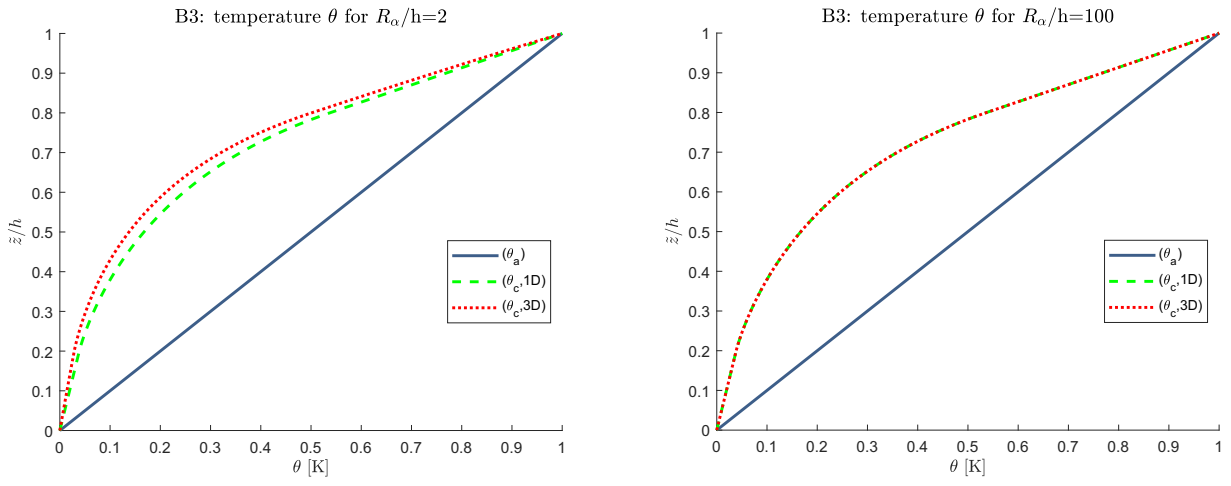

Figure 10: Third benchmark, temperature profiles for thick (on the left) and thin (on the right) sandwich cylindrical shell panel with FGM ($p = 0.5$) core. The maximum amplitude of the temperature $\theta(\alpha, \beta, z)$ is evaluated at ($a/2$,$b/2$).

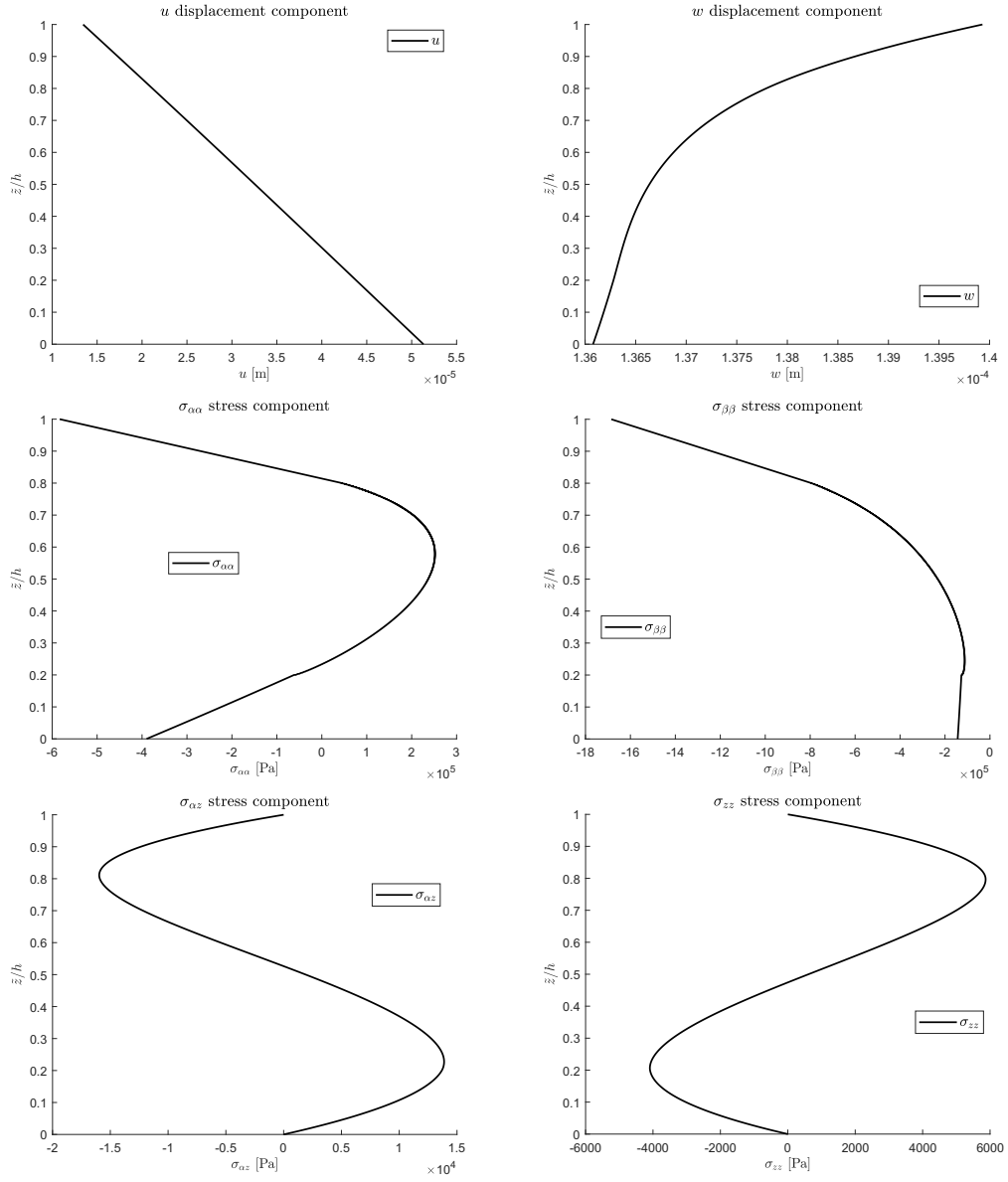

Figure 11: Third benchmark, displacements and stresses for thick (R_α/h=10) sandwich cylindrical shell panel with FGM ($p = 0.5$) core obtained via a 3D exact model based on a 3D calculated temperature profile 3D(θ_c,3D). Maximum amplitudes: u and $\sigma_{\alpha z}$ at (0,$b/2$); w, $\sigma_{\alpha\alpha}$, $\sigma_{\beta\beta}$ and σ_{zz} at ($a/2$,$b/2$).

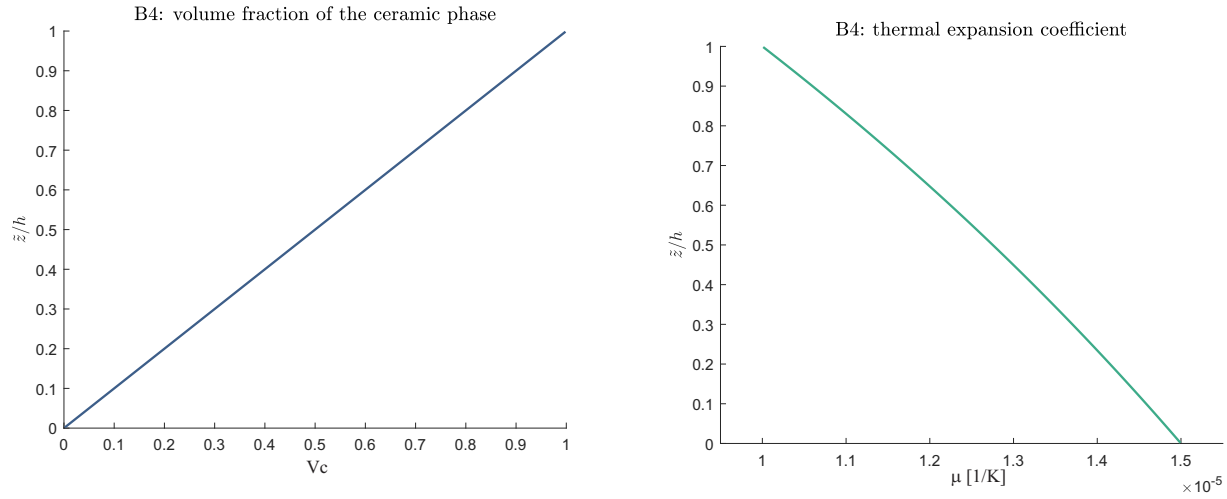

Figure 12: Fourth benchmark, volume fraction of the ceramic phase V_c (on the left) and thermal expansion coefficient μ (on the right) evaluated through the thickness of the one-layered FGM ($p = 1$) spherical shell panel.

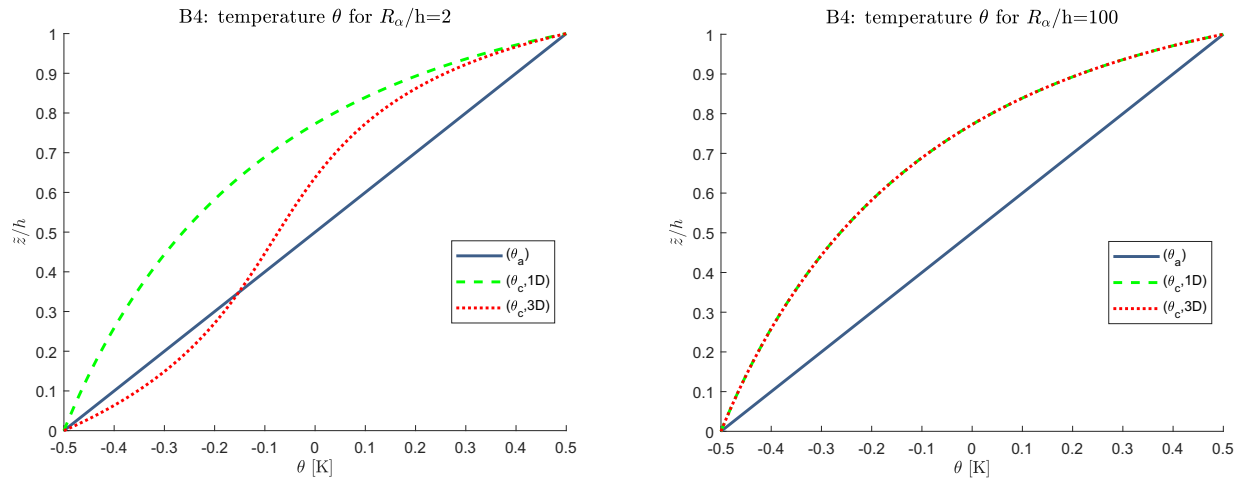

Figure 13: Fourth benchmark, temperature profiles for thick (on the left) and thin (on the right) one-layered FGM ($p = 1$) spherical shell panel. The maximum amplitude of the temperature $\theta(\alpha, \beta, z)$ is evaluated at ($a/2$,$b/2$).

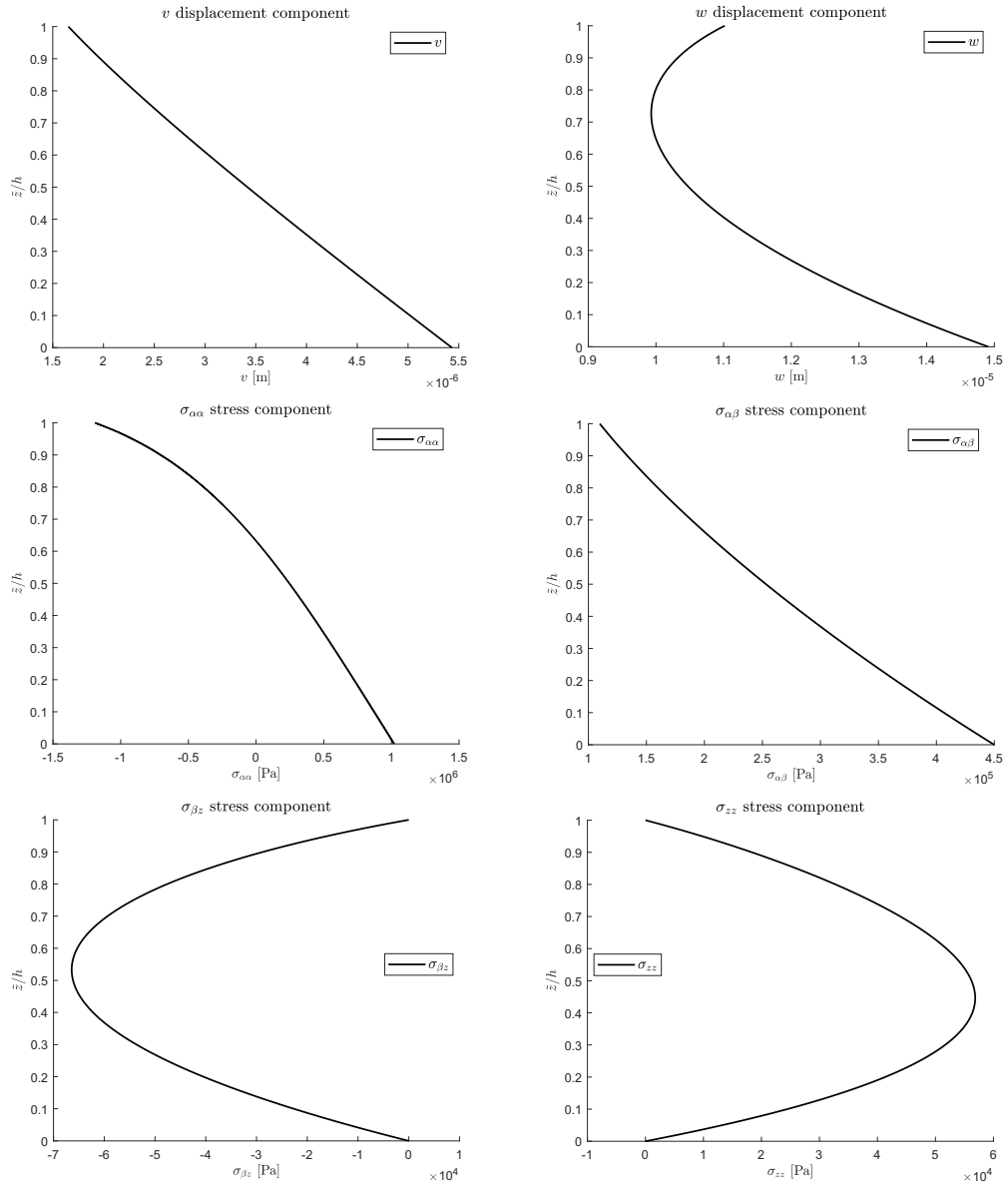

Figure 14: Fourth benchmark, displacements and stresses for thick (R_α/h=10) one-layered FGM ($p = 1$) spherical shell panel obtained via a 3D exact model based on a 3D calculated temperature profile 3D(θ_c,3D). Maximum amplitudes: w, $\sigma_{\alpha\alpha}$ and σ_{zz} at ($a/2$,$b/2$); v and $\sigma_{\beta z}$ at ($a/2$,0); $\sigma_{\alpha\beta}$ at (0,0).